HYPERSPECTRAL RADIOMETER & ULTRAVIOLET SPECTROMETER DESIGN

by

Vatsal Naik

Submitted in partial fulfilment of the requirements
for the degree of Master of Applied Science

at

Dalhousie University
Halifax, Nova Scotia
August 2016

DEDICATION

This thesis is dedicated to my parents, Jayeshkumar Naik and Alpanaben Naik, for their continued encouragement, support and best wishes.

Table of Contents

LIST OF FIGURES

ABSTRACT

Satlantic is currently developing a new hyperspectral radiometer for measuring spectral radiance in the ocean. This project includes the development of optical, mechanical, electronic, embedded firmware and software components in an integrated system and design of ultraviolet spectrometer. Initial steps included ultraviolet spectrometer design verification in simulation software and alignment of all components for calibration tests. Our research work also consisted laboratory evaluation of radiometer sensor components to determine polarization dependence, accuracy of wavelength, power consumption, linearity, sensitivity and temperature dependence.

LIST OF ABBREVIATIONS USED

C	Speed of Light
e	Electron charge
λ	Wavelength
UV	Ultraviolet
IR	Infrared
α	Incident Angle
β	Diffraction angle
m	Propagation-mode
G	Groove density
γ	Blaze angle
h	Plank constant
SI	Silicon
$InGaAs$	Indium gallium arsenide

$\boldsymbol{\lambda_m}$	Maximum wavelength
$\boldsymbol{Hg(Ar)}$	Mercury Argon
$\boldsymbol{Ne}$	Neon
$\boldsymbol{Xe}$	Xenon
$\boldsymbol{Kr}$	Krypton
$\boldsymbol{L_C}$	Focal length of collimating mirror
$\boldsymbol{L_F}$	Focal length of focusing mirror
$\boldsymbol{\omega_{slit}}$	Width of slit

ACKNOWLEDGEMENTS

I would like to express my sincere gratitude to my supervisor Dr. Michael Cada for his helpful guidance and encouragement throughout my graduate study. I express my appreciation to Dr. Jason Gu and Dr. William Phillips for being on my supervisory committee.

I would also like to thank Ronnie Van Dommelen, Keith Brown, Burkhard Plache and Scott Fenner for assisting me with my research during my Internship at SATLANTIC.

I am also very thankful to my lab mates for their selfless support. Special thanks to my numerous friends for their help.

Especially, I would like to give my thanks and love to my parents for their love and support for both my studies and in my personal life.

CHAPTER 1 INTRODUCTION

In this chapter, the overview of the thesis is presented, as well as, the motivation and objectives.

1.1 Overview

1.1.1 Hyperspectral Radiometer

The Pre-Aerosol, Cloud, ocean Ecosystem (PACE) mission is a recent addition to the NASA flight program [1,2]. The next generation of the PACE mission builds on previous ocean-color remote sensing efforts to provide global observation for understanding the living ocean and for improving skill in forecasting and projecting the variability of earth system over a range of time and space scales [3]. A Hyperspectral Radiometric device would provide accurate measurements of water leaving the radiance from autonomous platforms for satellite calibration [4,5]. A new Hyperspectral Radiometer system would be capable of meeting new requirements of spectral resolution (<3 nm), for observation in UV and near IR (350-900 nm), which will maintain accuracy, precision and stability of existing radiometers.

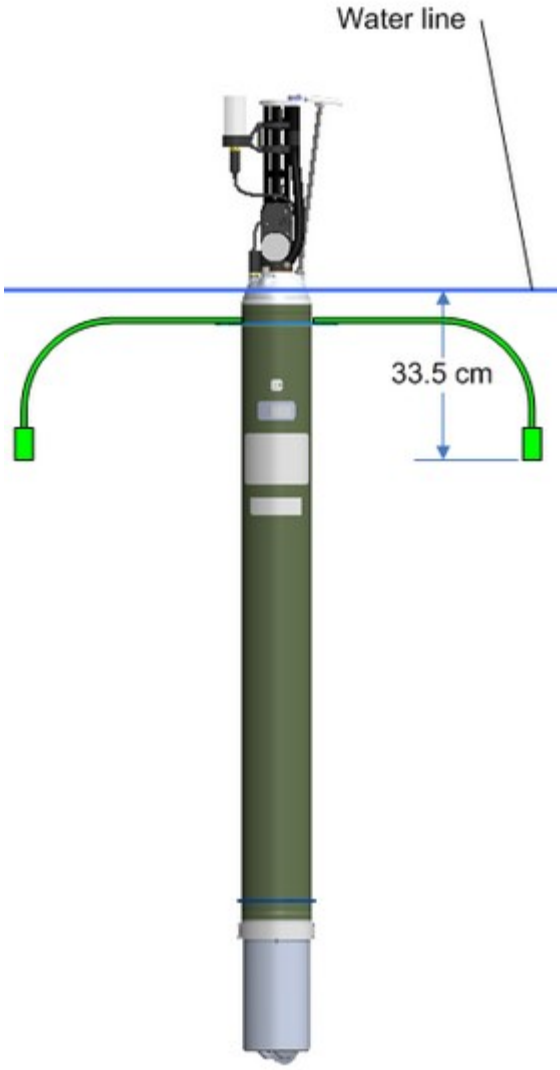

Figure 1.1 HyperNav Prototype Design

1.1.2 Basics of spectroscopy

A spectrometer can be used to measure the spectrum of light emitted from a source. A spectrometer must differentiate wavelengths. Prisms and Diffraction Gratings are two common options for differentiating wavelengths of light. Prisms distinct wavelengths due to the fact that glass has a refractive index, which depends on the wavelength. So, different

colors would be diffracted at unique angles. The diffraction grating origins multiple wavelengths of light to be diffracted at unique angles. Most spectrometers can be divided by the principle of operation into three groups.

- Fourier Transform Spectrometer: It uses a Michelson interferometer and a beam splitter to split light into two paths. To measure the intensity, the spectrum intensity function is produced. The technique can achieve a very high optical resolution.
- Spectrometer with a monochromater: This simply designed device has rotating diffraction grating. However, the device is less sensitive to the environment than other types of spectrometers. The most common setup for this device is the Czerny-Turner, but different geometries can be used for different purposes.
- Spectrometer with a multi-channel detector: It has no moving components. The grating is fixed and the spectrum is projected on a detector.

1.2 Motivation & Objective

The main motivation for our research project was to test the characteristics of spectrometers so we can meet the requirements for a hyperspectral radiometer. The objectives were:

1. To design a series of different tests which included the Lamp test, Polarization test, HeNe Laser test, Warm-up test, Linearity test and Thermal test.
2. Next objective was to design a low-cost, small UV spectrometer to improve the performance of an existing nitrate measurement sensor. It should be compatible with commonly available electronics and software.

3. After the design was ready, the next step was to start building a spectrometer design on an optical bench.

To meet our objectives, our first task was to design a spectrometer simulation. Then, we ordered the necessary mirrors, grating and holders. Our next step was to check the spectrum of calibration lamp with ISUS electronics and software.

1.3 Thesis Outline

The outline of this thesis is as follows. Chapter 1 introduces the project. Chapter 2 describes the main principle of diffraction and diffraction gratings. Chapter 3 introduces different configurations of spectrometer design. Chapter 4 lists the steps needed to design a UV spectrometer. At the end of Chapter 4, an optical bench setup is shown. In Chapter 5, the results of different experiments with spectrometers are shown to determine the characteristics of Hyperspectral Radiometer. Chapter 6 summarizes the conclusions drawn from the research project and offers suggestions for potential future work.

CHAPTER 2 THEORY

In this chapter, we will explain diffraction and diffraction gratings. At the end of this chapter, we will explain the ISUS testing board and calibration lamps that we used in our experiments.

2.1 Diffraction

Diffraction is the deviation of an electromagnetic wavefront from the path predicted by ray optics when wavefronts interact with a physical object such as an aperture or an edge. Diffraction manifests itself in the apparent bending of waves around small obstacles and the spreading out of waves past small openings. The Huygens-Fresnel principle can be used to describe the effects of diffraction. It states that every point on a wavefront generates a spherical wavefront and that each interferes to form a secondary wavefront. The figure below illustrates the Huygens-Fresnel principle applied to various wavefronts.

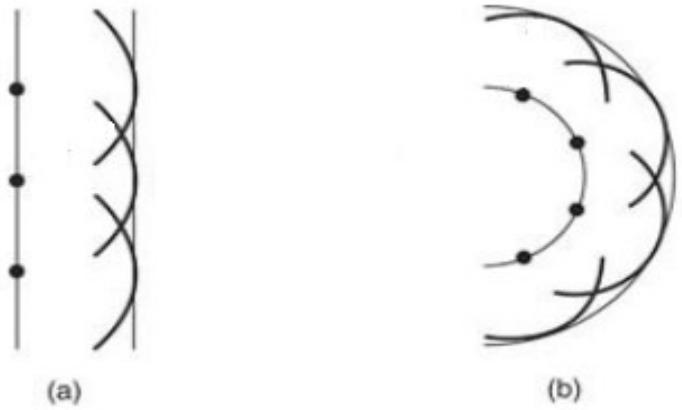

Figure 2.1 Huygens-Fresnel principle applied to (a) a plane wave, (b) a spherical wavefront. The black dots are point sources, and semi-circles are resulting wavefronts

2.2 Diffraction Grating

A transmission grating consists of a grating overlaid on a transmission surface, whereas a reflection grating consists of a grating overlaid on a reflective surface.

2.2.1 Grating Basics

When light is projected on a grating, it is diffracted. The reason is that each diffracting element acts as a point source, dispersing light in a spherical fashion as described by the Huygens-Fresnel principle. Due to more than one-point source, the phases of waves interfere with each other. When waves are in phase, they produce a bright intensity spot known as constructive interference. If the waves are out of phase, they produce a low-intensity spot known as destructive interference. Each bright spot is called a mode. For reflection gratings, if modes are on the same side of the grating, they are positive-ordered modes. Negative- ordered modes are on the opposite side of the grating normal.

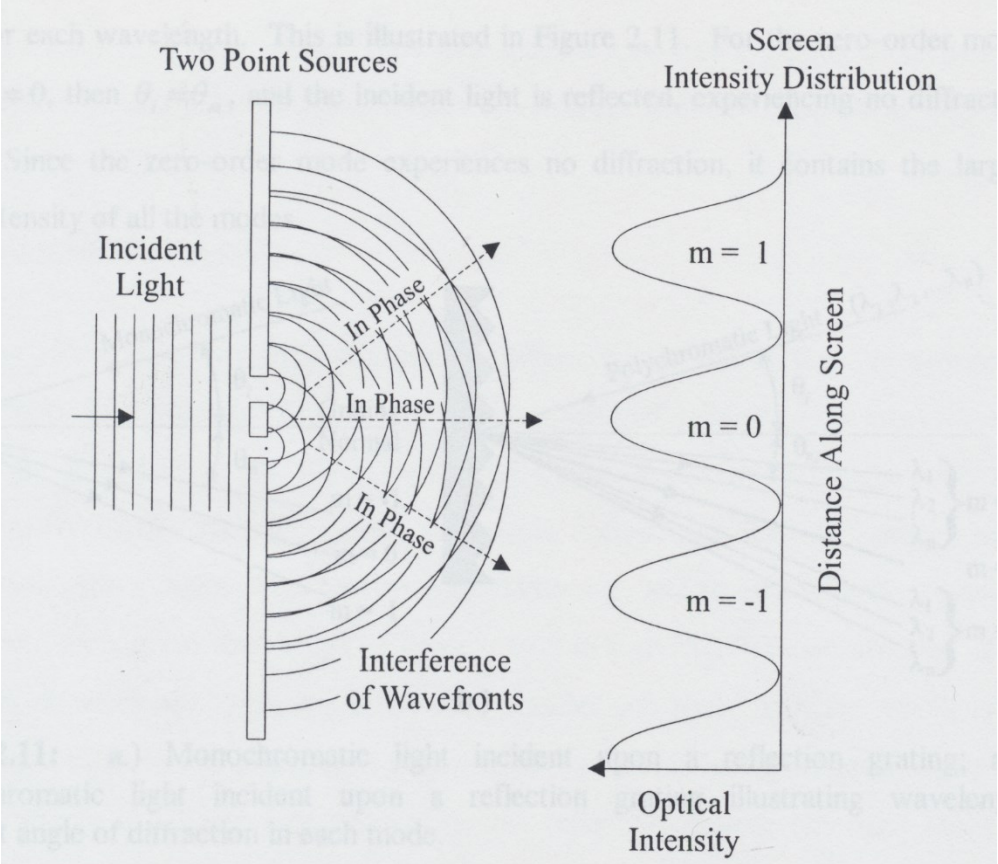

Figure 2.2 Two-slit grating and the far-field intensity pattern produced on a screen at the output of the slits. Where constructive interference occurs, it produces bright spots, called modes.

For a particular wavelength of light, the distance between the diffracting elements and the incident angle of the light determine the discrete angles at which the light will diffract.

2.2.2 The Equation of Grating

Grating surfaces diffract the incident light into different directions. A set of diffracted wavefronts forms by a combination of light diffracted by each groove. The usefulness of the grating depends on groove spacing d and the unique set of the discrete angler. The light

diffracted from each facet is in phase with other facet diffracted light that leads to constructive interference [6,7].

The figure below shows the light ray of wavelength λ incident at an angle α and diffracted by a grating at angles βm. Figure 1(a) shows reflection grating α > 0 and β1 > 0. Figure 1(b) shows the transmission grating.

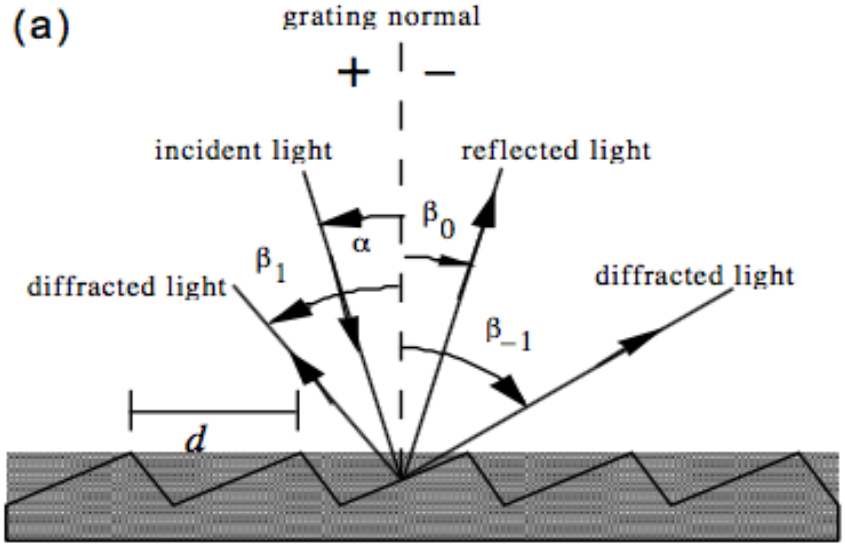

Figure 2.3 Reflection Grating diffraction [6]

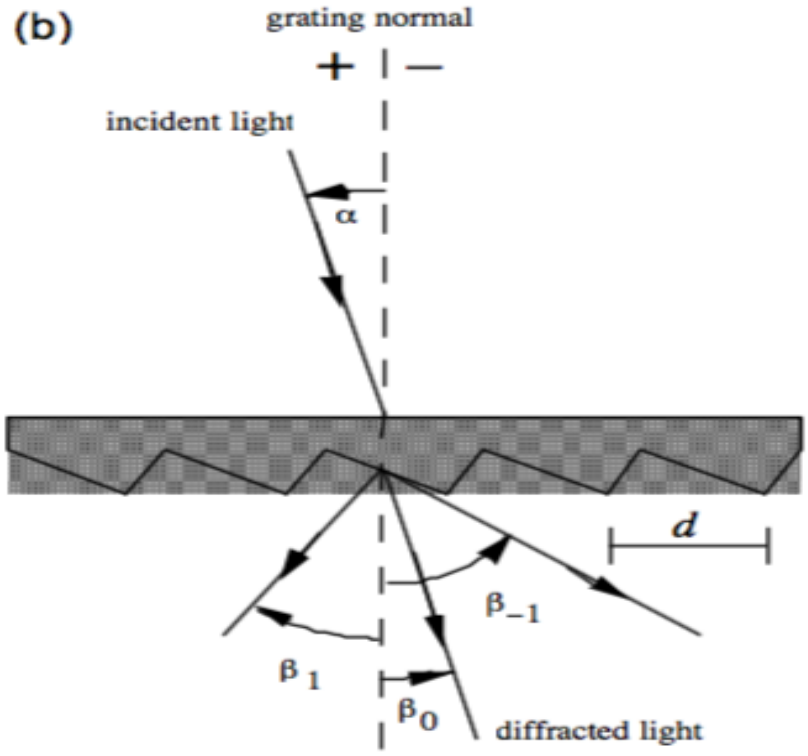

Figure 2.4 Transmission Grating Diffraction [6]

As shown by the arrows in the diagram, angles of incident and diffraction are measured from grating normal to the beam. In both diagrams, it is shown by plus and minus symbols.

Figure 2.4 shows grating diffraction using wavefronts. When geometrical path difference equals the wavelengths of light, it illustrates the principle of constructive interference. At all the other angles, the groove facets will interfere destructively. The grating equation are expressed by

$$m\lambda = d(\sin\alpha + \sin\beta) \qquad (2\text{-}1)$$

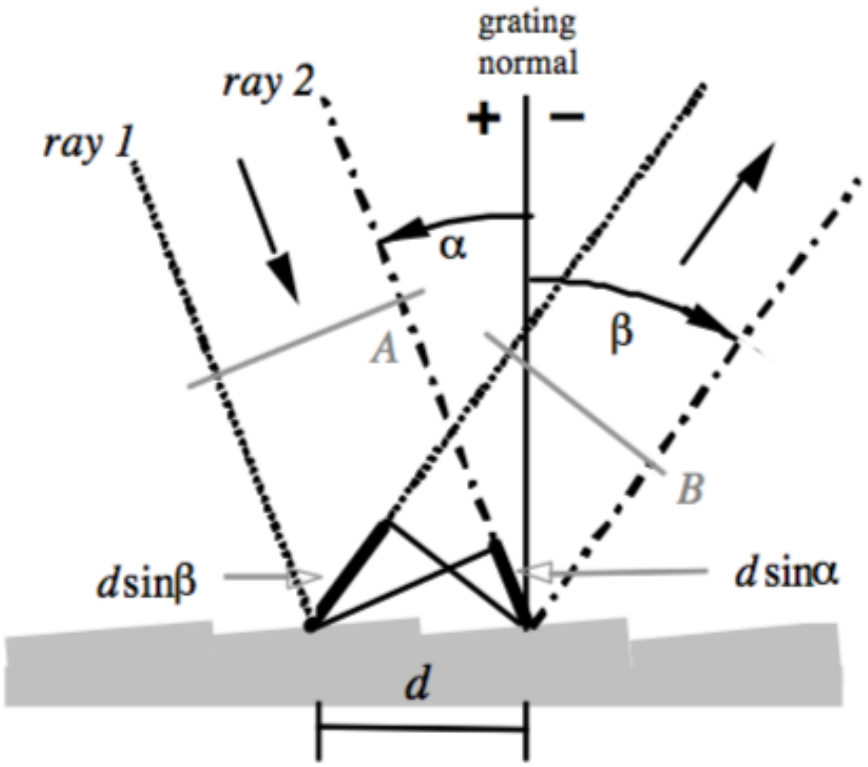

Figure 2.5 Geometry of diffraction for planer wavefronts [6,7]

The grating equation can also be written as follows:

$$G.m.\lambda = \sin\alpha + \sin\beta \tag{2-2}$$

Where, G = 1/d is the groove frequency or groove density

For a grating of groove density, there is a relationship between an angle of incident and diffraction. In a particular spectral order m, the different wavelengths of wavefronts incident at angle α are separated in angle:

$$\beta(\lambda) = \sin^{-1}\left(\frac{m\,\lambda}{d} - \sin\alpha\right) \tag{2-3}$$

When zero spectral mode grating acts as a normal reflecting mirror and wavelengths are not separated. This is called specular reflection or the zero order.

2.3 Littrow Configuration

The Littrow configuration plays an important role in spectrometer geometry. In this configuration, we can achieve the highest grating efficiency possible, with identical angles of incident and diffracted light: $\theta_i = \theta_m$ and $m > 0$.

$$m.\lambda_D = 2a\ \sin(\theta_L) \tag{2-4}$$

This configuration depends on the most intense order ($m = 1$), the wavelength and the grating spacing. The Littrow configuration θ_l is the same to the blaze angle γ at a particular wavelength.

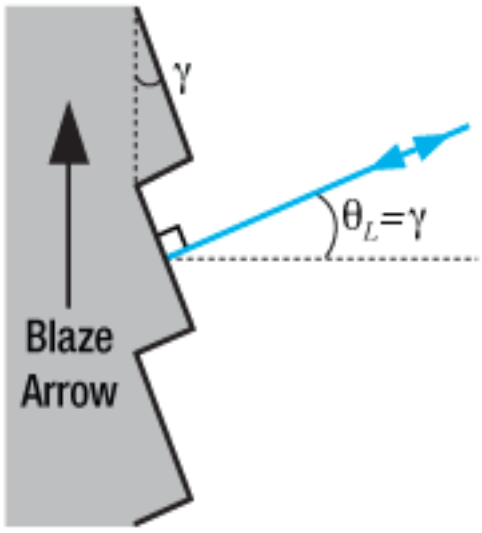

Figure 2.6 Littrow Configuration

2.4 Holographic Gratings

In the 1960s, researchers independently formed the first holographic diffraction grating [8].

While blazed gratings offer high efficiency at the design wavelength, they have drawbacks such as the high amount of scattered light, which decreases spectral sensitivity. The gratings we used were designed to reduce these errors.

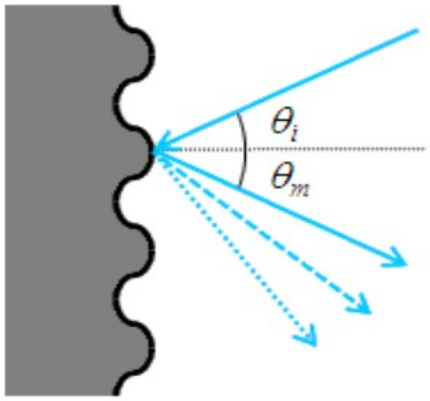

Figure 2.7 Holographic Gratings [8]

The manufacturing process of these gratings is different than the process used for ruled gratings. In the process we used, photosensitive material was exposed to two interfering lasers. The interference design pattern was exposed on the surface, then, either physically or chemically processed to form a sinusoidal pattern.

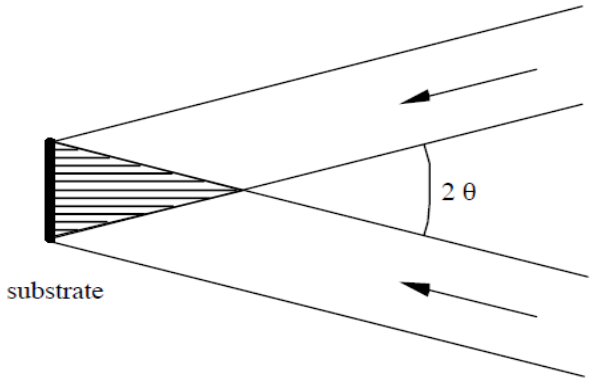

Figure 2.8 Formation of interference fridges [8]

2.5 Difference between Ruled and Holographic Gratings

Ruled and Holographic gratings each have pros and cons due to differences in their fabrication processes. Some of them are described below:

I. Differences in efficiency

The efficiency of ruled and holographic gratings differs considerably, due to differences in the groove patterns, but not due to the different manufacturing processes. For ruled and holographic gratings, there is no rule for describing the efficiency curve difference.

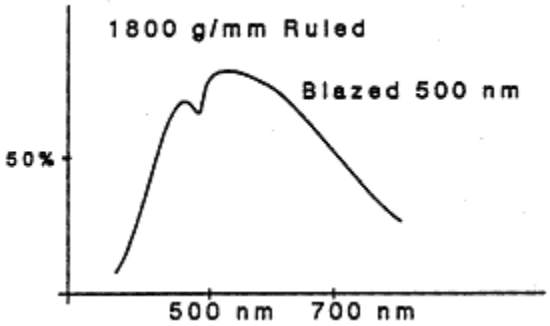

Figure 2.9 Efficiency of Ruled grating [11]

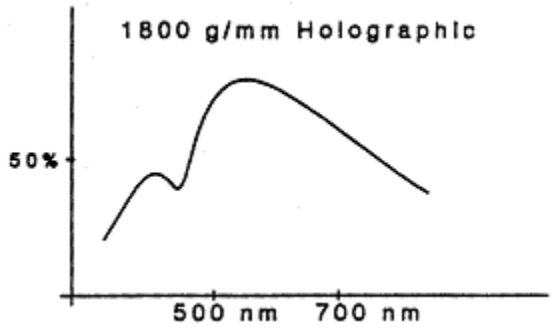

Figure 2.10 Efficiency of Holographic grating [11]

II. Differences in scattered light

The surface irregularities on the grooves of Holographic gratings differ from ruled gratings. In the study of Raman spectra of solid samples, the Holographic grating can offer advantages. But for Holographic gratings, stray light from other sources must not be present because it can affect the performance of the gratings.

III. Limitations in obtainable groove frequencies

Ruled and Holographic gratings both offer different grooves per millimeter ranges. Ruled gratings offer a range of groove spacing compared to Holographic gratings. At a lower limit, a few hundred grooves per millimeter are necessary to generate Holographic gratings while Ruled gratings can have less than fifty grooves per millimeter. At a higher limit, both types of the grating can be produced with several thousand grooves per millimeter.

IV. Difference in groove patterns

Normal Ruled gratings, the most common type of gratings, have straight, equally spaced grooves. Holographic gratings need not have straight grooves. According to the required

optical resolution, the curvature of grooves can be modified. This pattern can significantly improve the imaging of a system whereas classic Ruled gratings require some auxiliary optics.

V. Difference in the size of the substrate

Ruled gratings can be as large as Holographic gratings with physical dimensions of as much as 320 x 420 mm.

VI. Difference in Manufacturing time

In Ruled gratings, each groove is formed individually; to do so, a ruling diamond may travel a long distance. For example, a Ruled grating with the dimension of 100 x 100 mm and with 1,000 groove density will require a diamond to move 10km which may take many weeks.

In the case of Holographic gratings, grooves are created simultaneously. The time it takes may vary from a couple of minutes to tens of minutes, which depend on the intensity of the laser and the spectral response of photoresist at this wavelength. If we add preparation and manufacturing time, the production time for Holographic gratings is much less compared to Ruled gratings.

2.6 Concave Gratings

Many grating applications use a plane grating with lenses and mirrors to separate spectral components of the source. A concave grating can be formed as a concave mirror; it can focus light by virtue of its concavity [7,12]. Concave gratings have an advantage over

conventional gratings because they perform both imaging and wavelength-separation tasks. This reduces alignment time as well as reflective or refractive energy losses. Concave gratings are critical components in a variety of spectroscopic instrumentation. Advanced design and manufacturing techniques used in production increase performance of the concave gratings.

In the past, hyperboloids were used to form grooves on the grating surface. When projected, these grooves show both unequal spacing and curvature. While in second generation light from sources transmitted through lenses or reflected by concave mirrors, so the recording wavefronts are toroidal [14].

2.7 Spectral Resolution

Spectral Resolution, also called optical resolution, shows the important characteristics of a spectrometer. It determines a maximum number of spectral picks that a spectrometer can resolve. For example, a spectrometer with a wavelength range of 250nm and a spectral resolution of 1nm would be capable of resolving as many as 250 individual wavelengths across a spectrum.

The slit, the detector and the diffraction grating are the main components that affect the resolution of a spectrometer. The slit determines the image size forming on the detector plane. The total wavelength range of the spectrometer depends on the diffraction grating. The detector decides the number and the size of a discrete point in which the spectrum can be digitized.

2.8 Polarization

Polarization refers to a plane of vibration of the light wave. It occurs when the source does not produce polarized light, but it can become polarized if it bounces off a surface at a glazing angle or it passes through an object that restricts the direction of vibration. The figure below shows light passing through a polarizer.

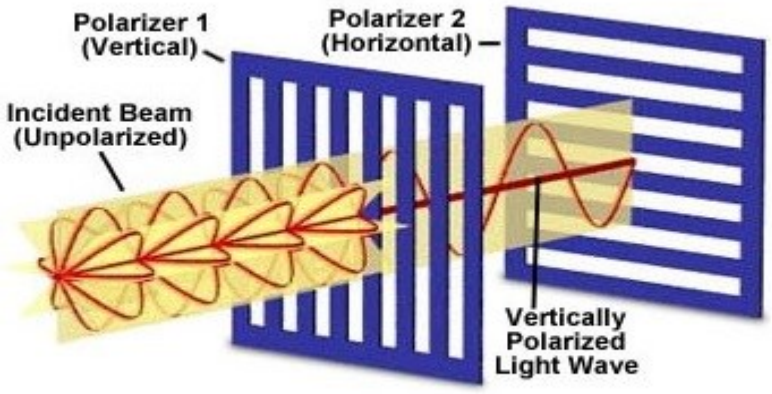

Figure 2.11 Light Passing through polarizer [16]

2.9 ISUS Test JIG

Satlantic's ISUS is a real-time nitrate sensor. It uses nitrate absorption technology to provide accurate measurements of nitrate concentration in a sample. The ISUS test jig is used to check the performance of ISUS's main assemblies (UV lamp, spectrometer and probe). The figure below shows the overall test jig layout [17].

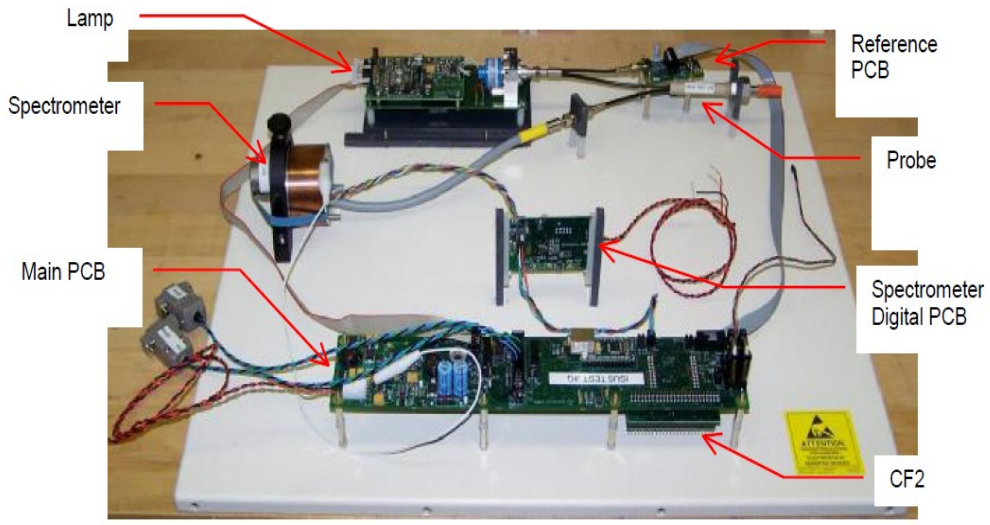

Figure 2.12 ISUS Test jig layout [17]

The new design spectrometer will replace the existing ISUS spectrometer. The figure below shows the current spectrometer of ISUS.

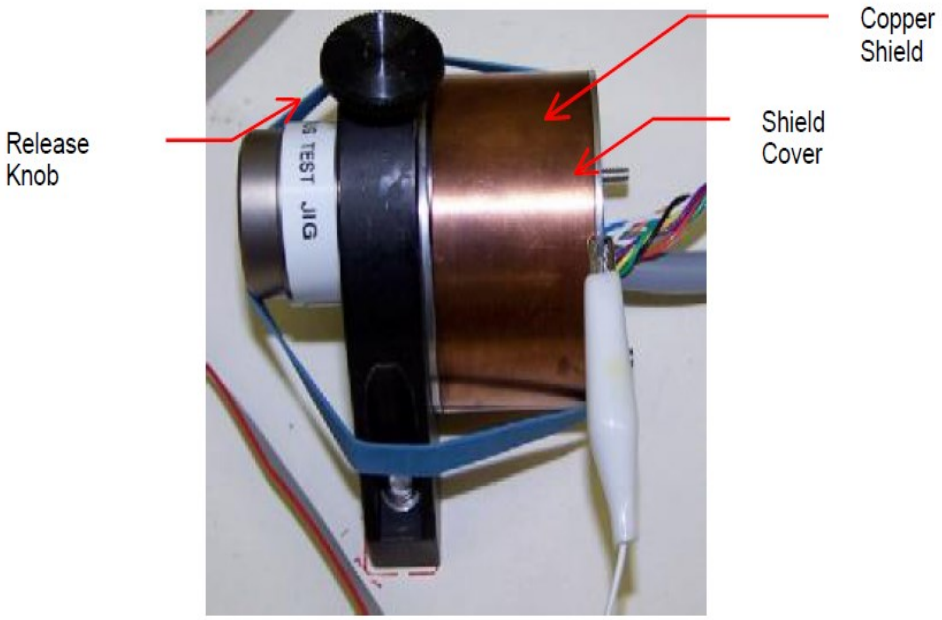

Figure 2.13 ISUS Current Spectrometer [17]

2.10 Detector Array

A detector array is a linear array of discrete detectors on an integrated circuit chip. As the diffracted light is captured by the individual pixels of the detector, each pixel represents the bit range of the spectrum that electronics will display with a given intensity using software. A photodetector can be differentiated from other detectors in many ways, most notably, by what material was used to make it. It can be Si and InGaAs array. It is important to choose the proper material when designing a spectrometer because bandgap energy (E_{gap}) of the semiconductor determines the λ_{max} that can be detected by the following relationship.

$$\lambda \max = \frac{hc}{\text{Egap}} \tag{2-5}$$

Where h is plank's constant and c is a speed of light. For example, band gap energy of Si is 1.11eV which gives a maximum wavelength of 1117.117nm. On the other hand, InGaAs is an alloy with band gaps of 0.36eV and 1.43eV respectively. The bandgap energy depends on the ratio of In and Ga. Furthermore, due to a number of other factors, it is not possible to fabricate all possible ratios of In and Ga.

For our application, we used the current ISUS detector array which was removed from one spectrometer, so we could use the existing electronics and software of Satlantic. The Figure 2.14 shows the detector array connection.

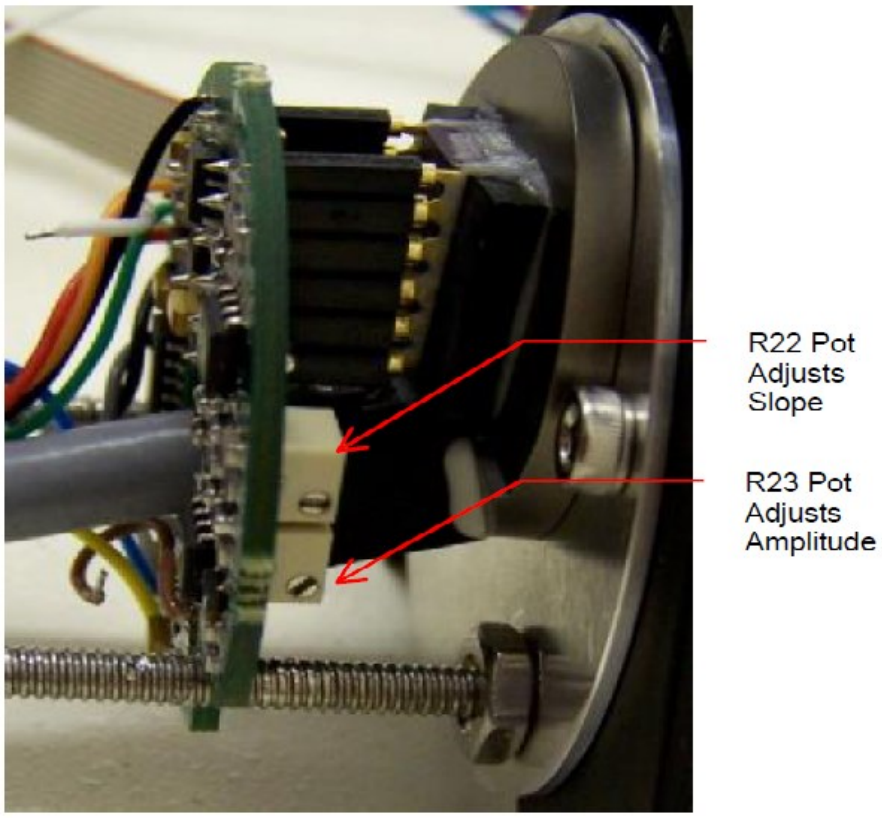

Figure 2.14 ISUS detector array connection [17]

2.10.1 MPP Mode

In the spectrometer B graph, the dark counts are high. To resolve that problem, we used another operating mode known as multi-pinned phase mode (MPP). Figure 2.16 shows the comparison of MPP mode and non-MPP mode. Different lines indicate dark counts for different integration times.

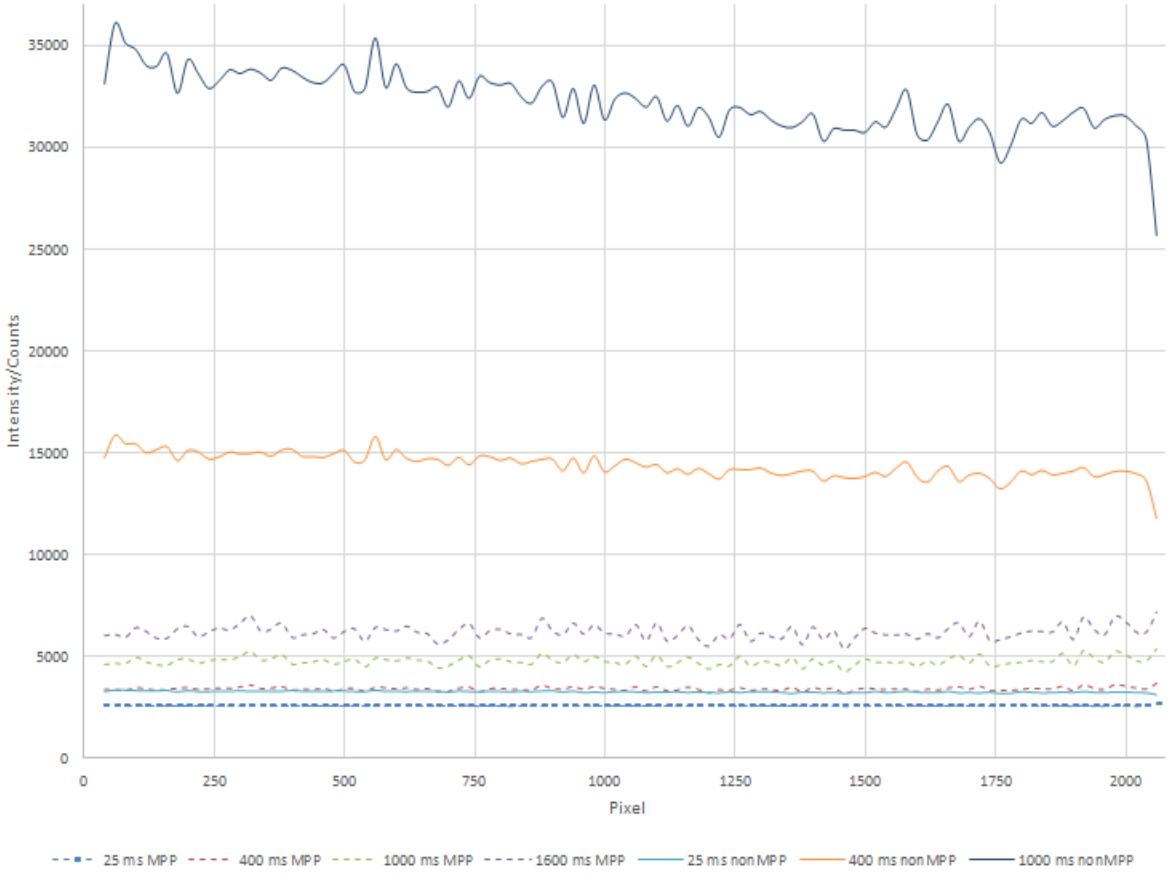

Figure 2.15 MPP mode dark counts for various integration time

MPP mode is applied to the CCD by biasing array clocks negatively which results in an invert n channel. That affects holes from the p channel prevents to migrate the populate silicon interface, eliminating the surface dark current generation [18].

Hence, this mode has one disadvantage since the potential wells within a pixel all assume the equal level the CCD full capacity annihilated since the wells within a pixel assume an equal level [18].

2.11 Light Source

2.11.1 FEL Lamps

Fluorescent electroluminescent lamps are popular for an application where a high stability with a wide spectral range light source is needed without sharp spectral lines. These lamps are available with the option of a benefit; NIST (National institute of Standards and Technology) traceable calibration. This NIST-traceable light source allows a user to calibrate spectroscopic system in lamp [19]. Figure 2.16 shows an image of FEL lamp.

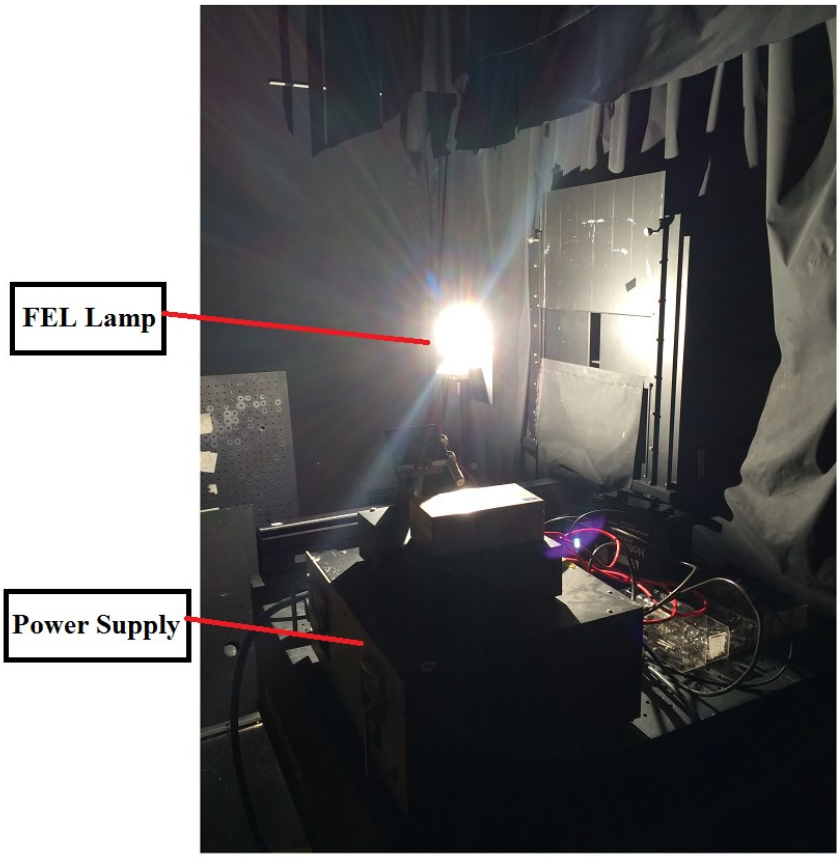

Figure 2.16 FEL Lamp

2.11.2 Calibration Lamps

A calibration lamp is a Rare Gaslamp (Argon, Krypton, Neon or Xenon gas) used for wavelength calibration of a spectrograph. These lamps produce narrow, intense lines of ultraviolet to infrared wavelengths due to excitation of different metal vapors and gasses.

These lamps are often used for calibrations because of their constant and repeatable average intensity [20]. Also, these lamps are insensitive to temperature after a warm-up stabilization period. The spectrum of these lamps is shown below.

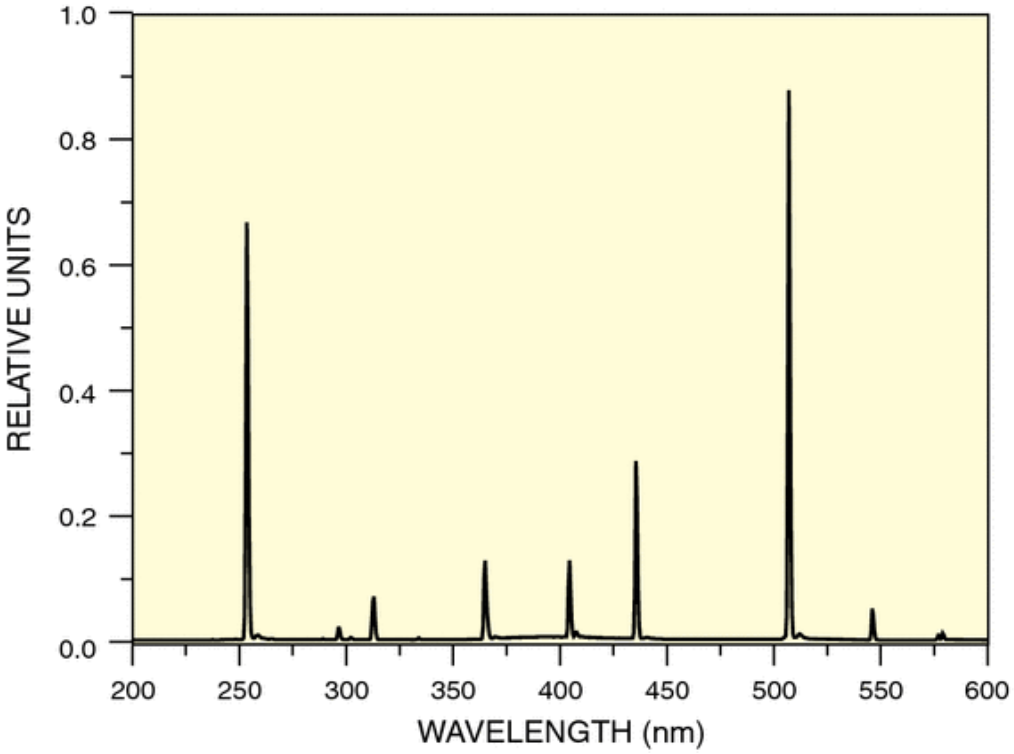

Figure 2.17 Mercury(Argon) lamp spectra [20]

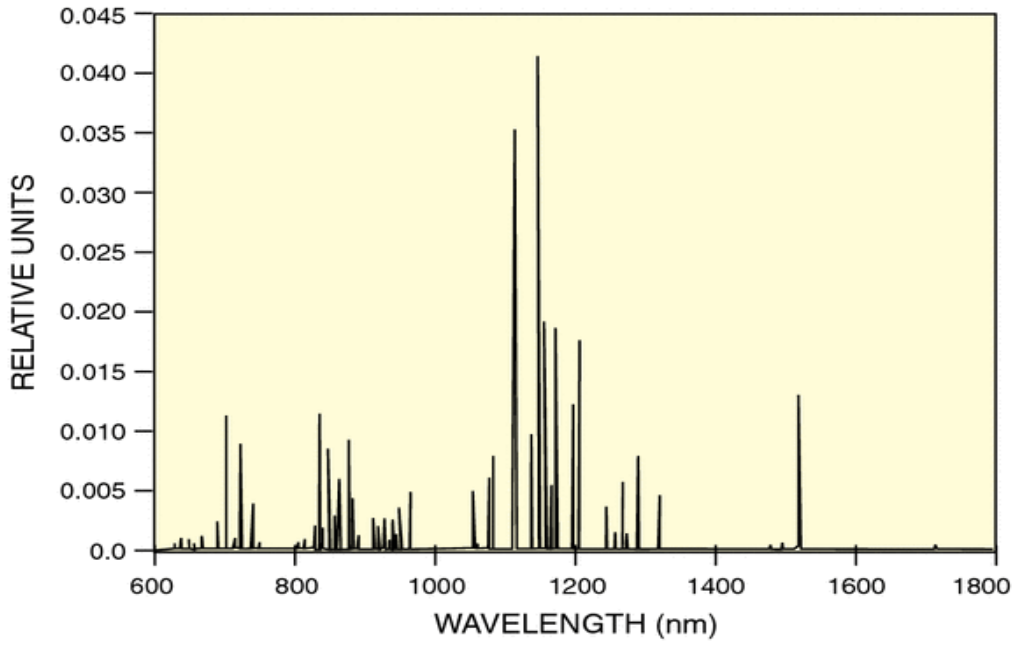

Figure 2.18 Neon lamp spectra [20]

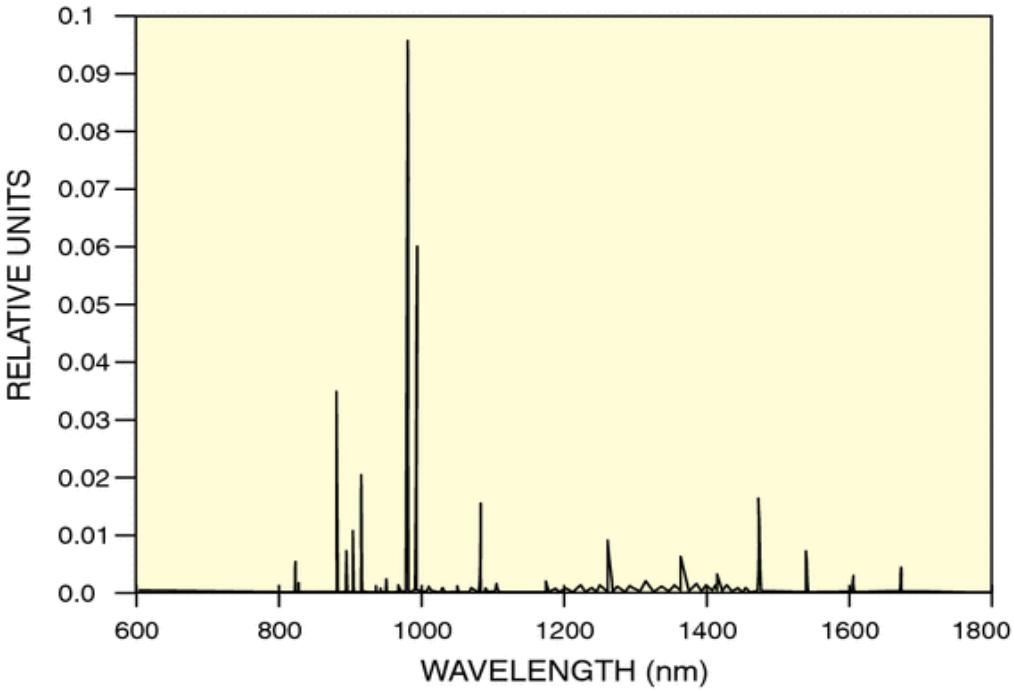

Figure 2.19 Xenon lamp spectra [20]

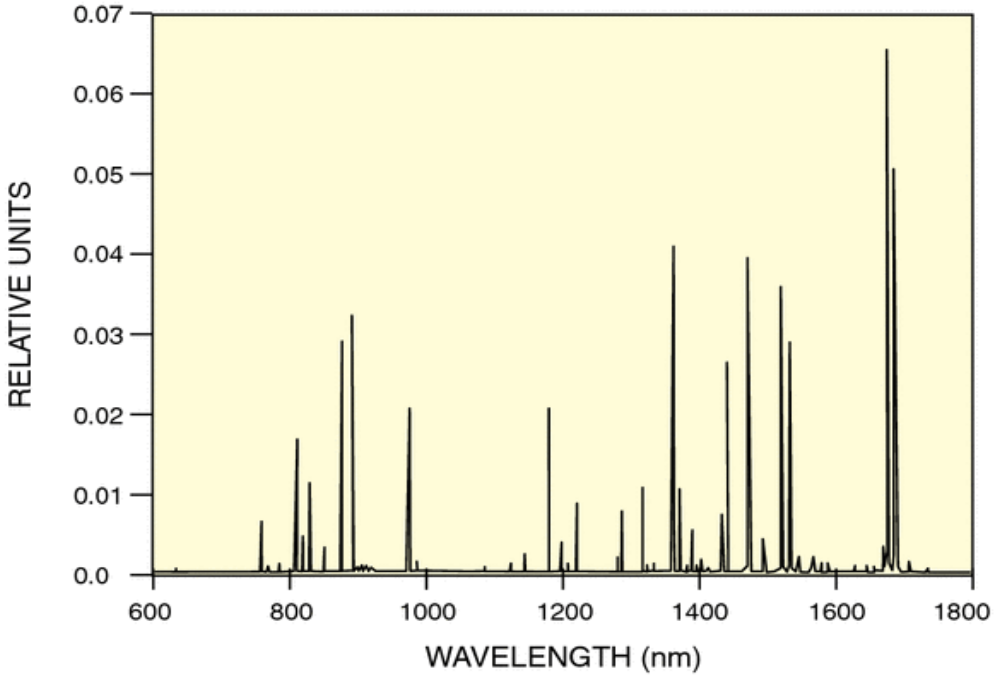

Figure 2.20 Krypton lamp spectra [20]

CHAPTER 3 Different Spectrometer Design

At the beginning of this thesis, we discussed the slit, diffraction grating and detector, which are the key components of a spectrometer. This chapter will explain the different ways to use these components to build a system. There are many possible configurations to build a spectrometer but the most popular types are the Czerny-tuner and the concave holographic spectrograph.

3.1 The Czerny-Tuner monochromater [21-23]

3.1.1 Cross-Czerny Tuner

The Czerny Tuner design contains of concave mirrors and a diffraction grating. The focal length of mirror 1 is selected in such way that it focuses all the light coming from the entrance slit and leads it toward the diffraction grating. Once the light is diffracted from the diffraction grating, another concave mirror is used to focus all light to the detector plane. Figure 3.1 shows the crossed Czerny-tuner spectrograph.

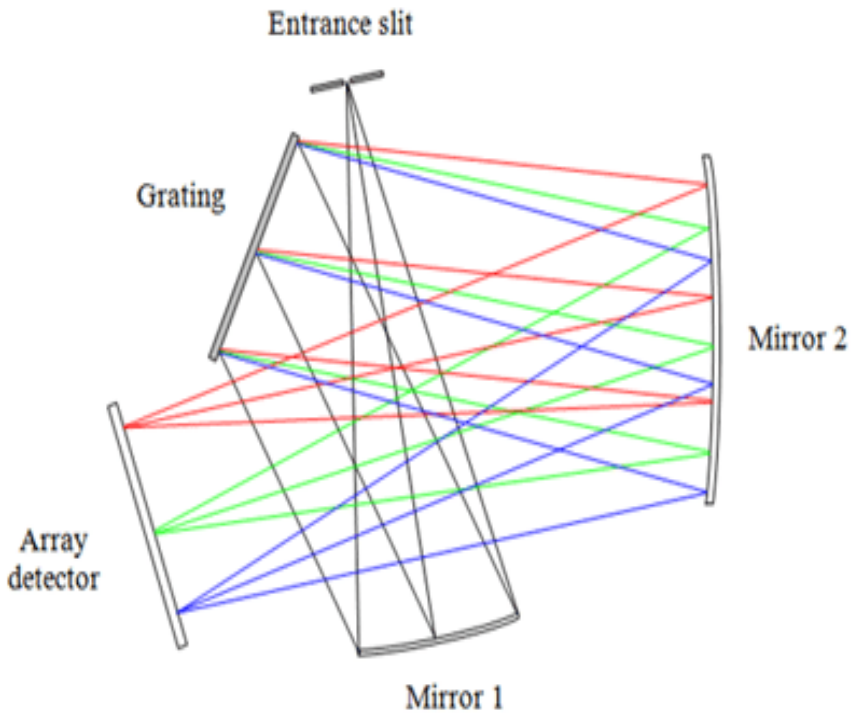

Figure 3.1 Crossed Czerny-Tuner Spectrograph [24]

The main advantage is it offers compact and flexible design. However, due to its off-axis geometry, this configuration is primarily used for lower resolution spectrometers.

3.1.2 Unfolded Czerny-Tuner

To minimize image aberrations, the unfolded Czerny Tuner is designed with an f-number >3. The large f/# of the Czerny-Tuner design can result in high levels of stray light in the system. One simple and cost-effective way to reduce stray light in the system is to change the design. Figure 3.2 shows an unfolded optical bench which allows us to insert a beam block in the optical path to reduce stray light.

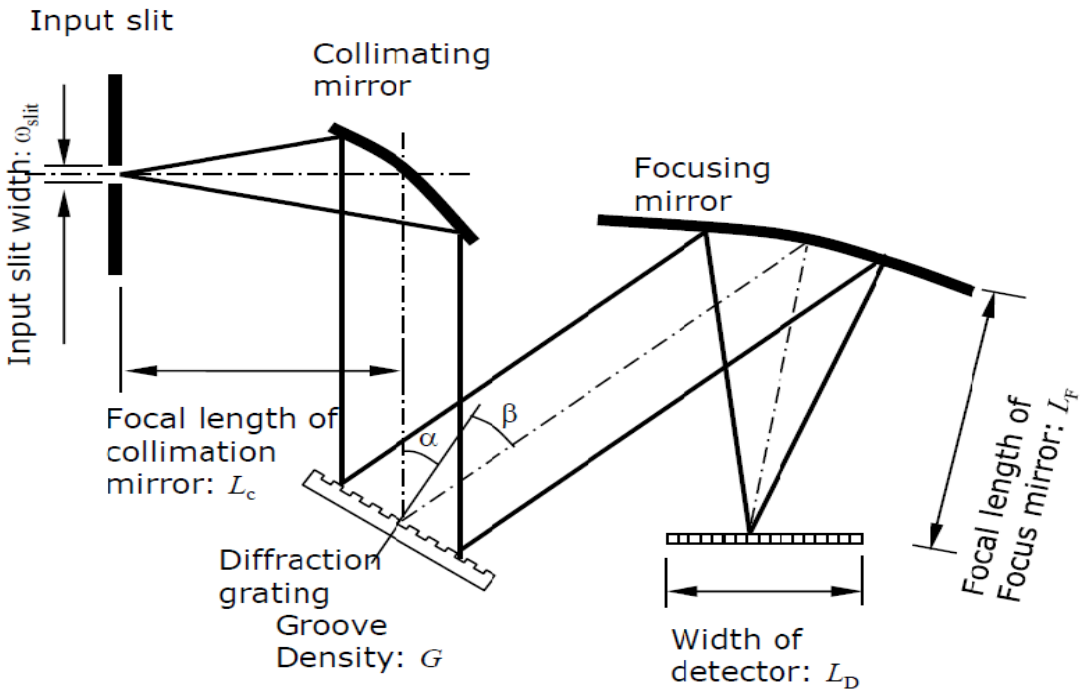

Figure 3.2 Unfolded Czerny-Tuner Spectrograph

1. **Choose Geometry:** The first step is to select geometry.

$$\phi = \alpha + \beta \tag{3-1}$$

2. **Choose Grating:** The next step was to select diffraction grating according to the application being used. In this case, we chose grating that has high diffraction efficiency in our desired wavelength. Then we selected groove density. We chose diffraction grating from THORLAB (GH13 – 06U) which has a groove density of 600 grooves/mm. The dimension of our grating was 12.7mm x 12.7mm x 6.0mm (W x H x D).

3. **Calculation of Angle:** The incidence angle and angle of diffraction are the key parameters in the design of a spectrometer. After the grating density G is chosen these two angles can be calculated by using this Equation:

$$\alpha = \sin^{-1}\left(\frac{\lambda_c G}{2\cos\frac{\phi}{2}} - \frac{\phi}{2}\right) \quad (3\text{-}2)$$

4. **Detector Selection:** The purpose of the optics in a spectrometer is to diffract the light and focus it to the width of the detector array $L_{D.}$ There are many kinds of detector arrays available in the market. For this test, we used the current detector array from ISUS which was an ideal choice for an initial design.

5. **The focal length of mirrors calculations:** Once the width of a detector is known, the focal length of the focusing mirror can be calculated.

$$L_{f=\frac{L_D\cos(\beta)}{G\,(\lambda_2-\lambda_1)}} \quad (3\text{-}3)$$

The equation below helped us select the focal length of the imaging mirror.

$$L_c = L_f \frac{\cos(\alpha)}{m\cos(\beta)} \quad (3\text{-}4)$$

6. **Input Slit:** The input slit width is determined by the required optical resolution DI and the magnification. For our application, we bought one from National Aperture: 100umx3mm, 25mmØ, mounted Part No: 2-100-3, National Aperture.

$$\omega_{slit} = \frac{G.\Delta\lambda.L_c}{\cos(\alpha)} \quad (3\text{-}5)$$

Figure 3.3 shows the inside view of the spectrometer.

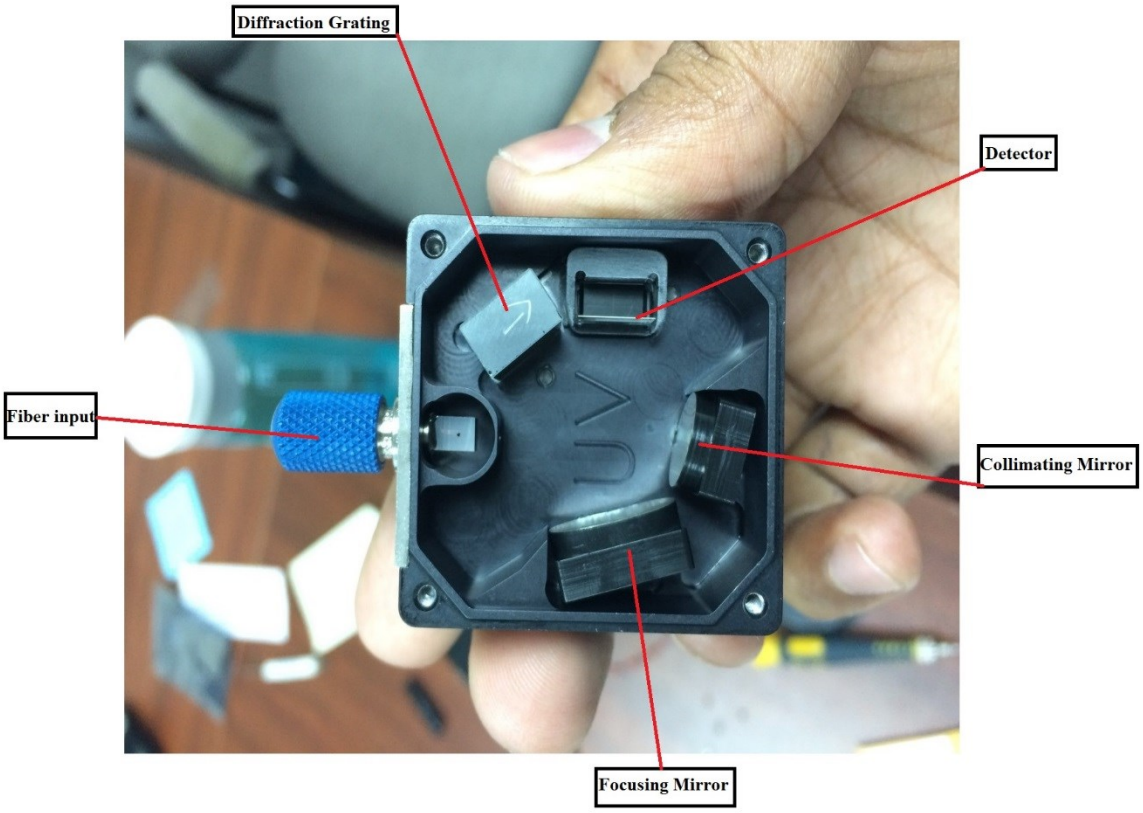

Figure 3.3 Inside view of a spectrometer

3.2 Concave Holographic

The other most popular optical bench design is based on the concave holographic grating. Here, the concave grating is used to eliminate dispersive and a focusing mirrors which also reduces optical components in the system. The concave design allows up to 10 times the reduction in stray light than the normal ruled grating design.

CHAPTER 4 UV Spectrometer Design

In this chapter, we will show the steps to design the Czerny-Tuner setup in COMSOL software. We will also include the optical bench setup with alignment and calibration lamp output in SetView software.

4.1 Software Introduction

4.1.1 COMSOL Multiphysics

COMSOL Multiphysics is a finite element analysis and simulation software for various physics and engineering applications [24-26]. We used a Ray-optics module for our design simulation.

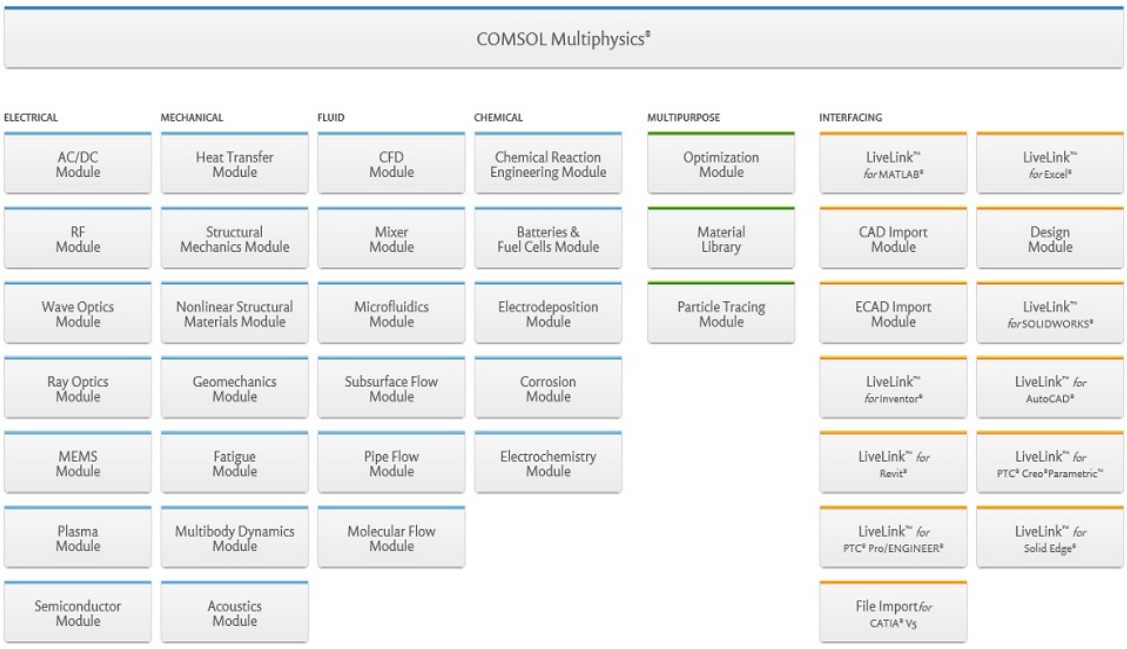

Figure 4.1 COMSOL Module [24]

4.1.2 Zemax

Zemax is one of the most popular optical design programs for Microsoft Windows sold by the American Company Zemax LLC [27]. It is used for the design and analysis of imaging and illumination systems. It can import non-sequential elements from CAD software as well as export to CAD software, in particular, SolidWorks. Furthermore, it has a huge database which makes it quick and easy to find solutions to specific problems.

4.1.3 SetView

SetView is a data display and logging application for use with Satlantic radiometers. SetView provides direct serial communication with instruments, real-time graphical display of data, custom log files, as well as, spectral views and details about all the sensors attached to radiometers [28].

4.2 Software Design

Any software design needs basic parameters to be set. The parameters in this case will define the positions of all mirrors, gratings and detector arrays. In COMSOL, we needed to build dimensions according to our requirements and then, we defined surface properties such as groove density for gratings, etc. Please refer to Chapter 3's designing equations to see how we calculated wavelength range, the focal length of imaging and focusing mirrors, and angle of reflections, etc.

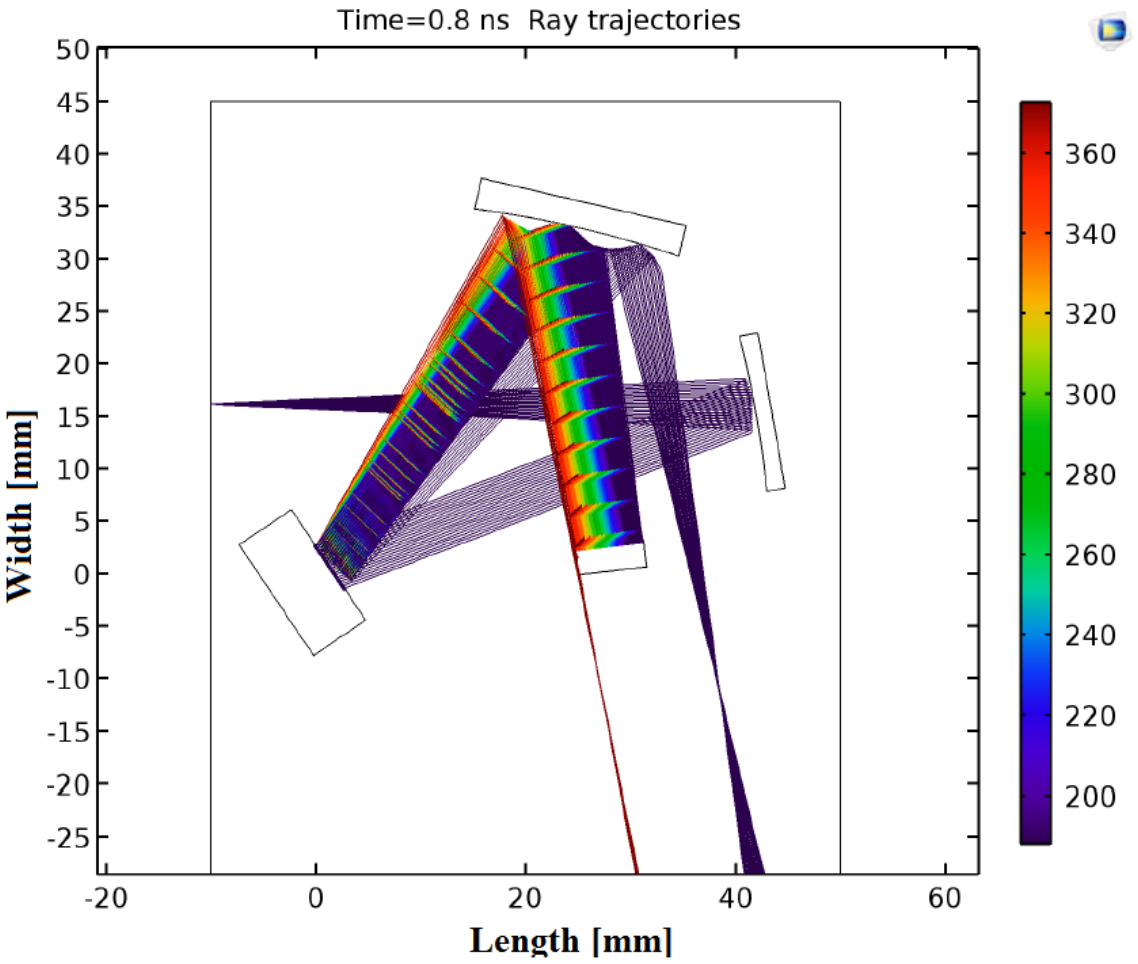

Figure 4.2 Design in COMSOL Multiphysics

Figure 4.2 shows the design in COMSOL software. In Both the X and Y axis, we represented the physical dimensions in mm. On the right side, we used different colors to show wavelengths in nm. Also, we used Zemax software because of its compatibility with SolidWorks software.

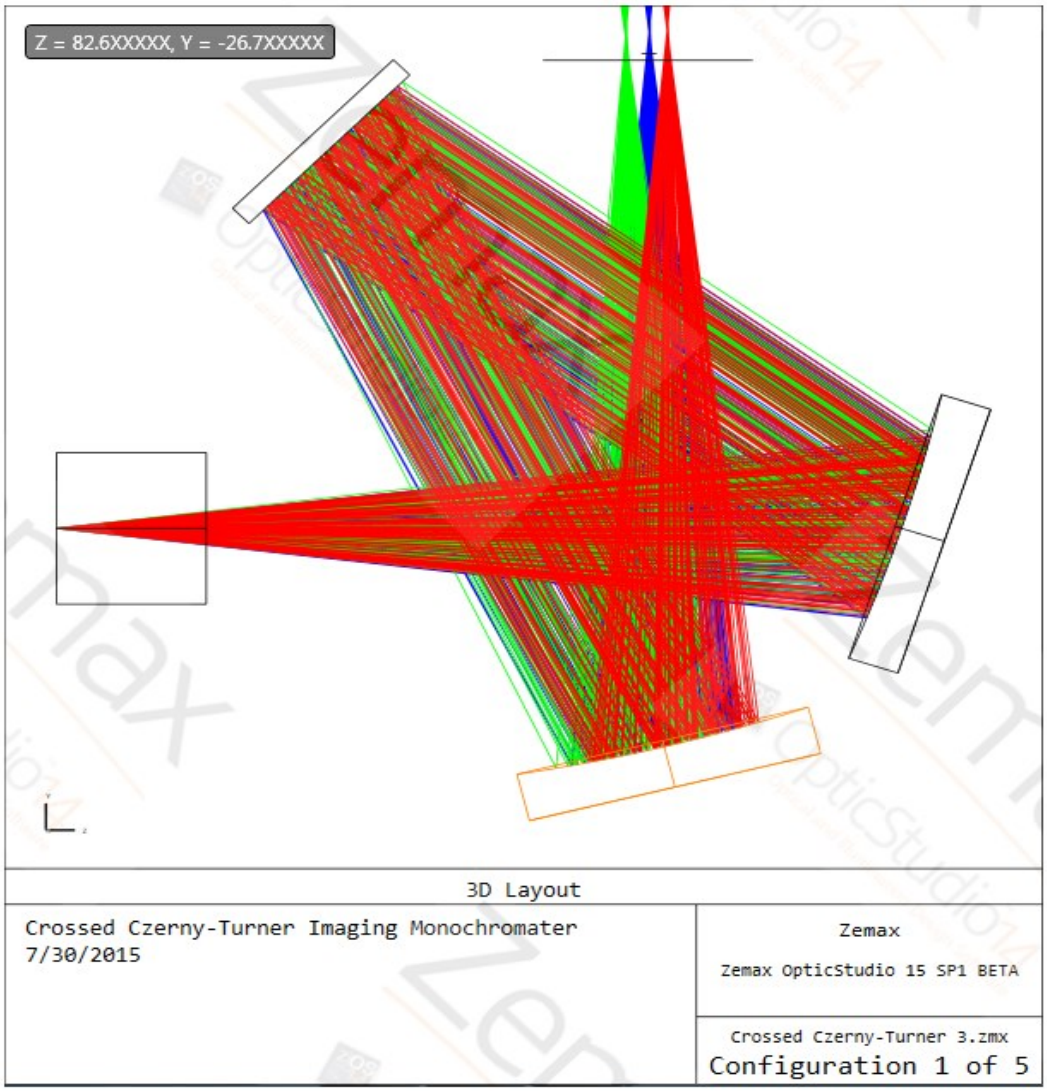

Figure 4.3 Design in Zemax

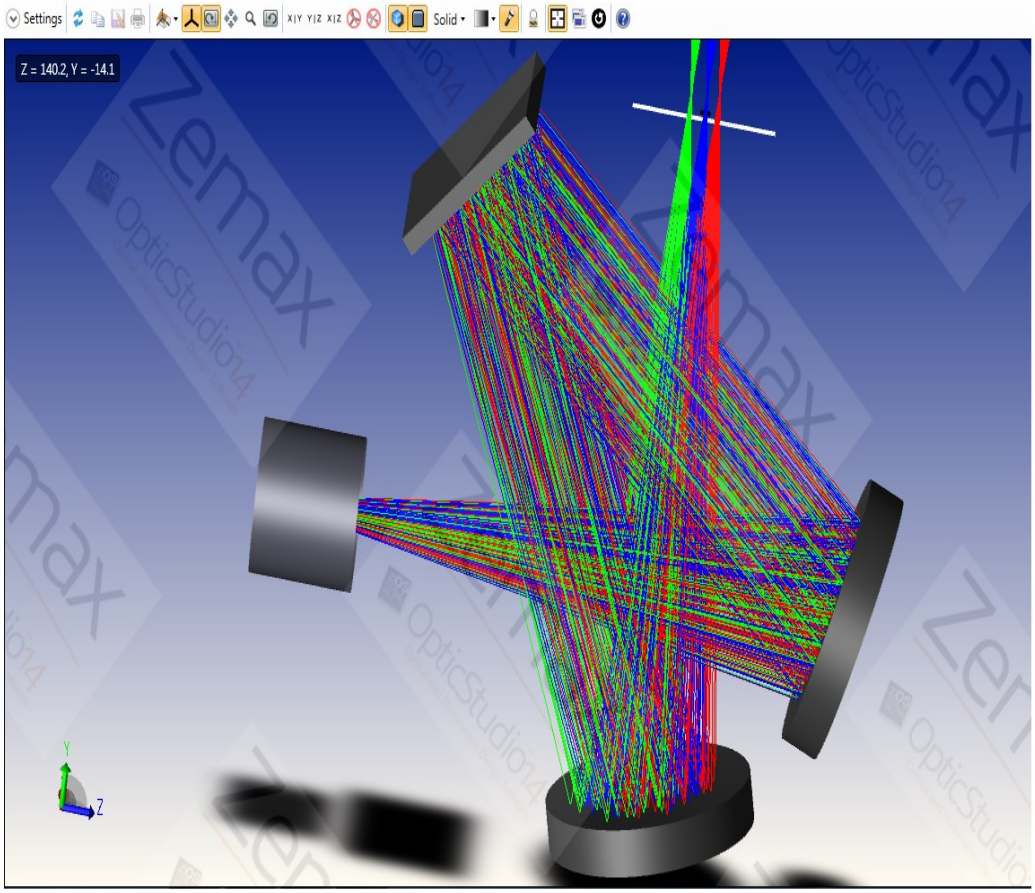

Figure 4.4 Zemax 3-D design

4.3 Optical Bench Setup

After designing using simulator software, we built a spectrometer on an actual optical bench. We changed dimensions a couple of times because we were testing it on the optical bench. The image below shows the bench setup with all optics placed with their holders.

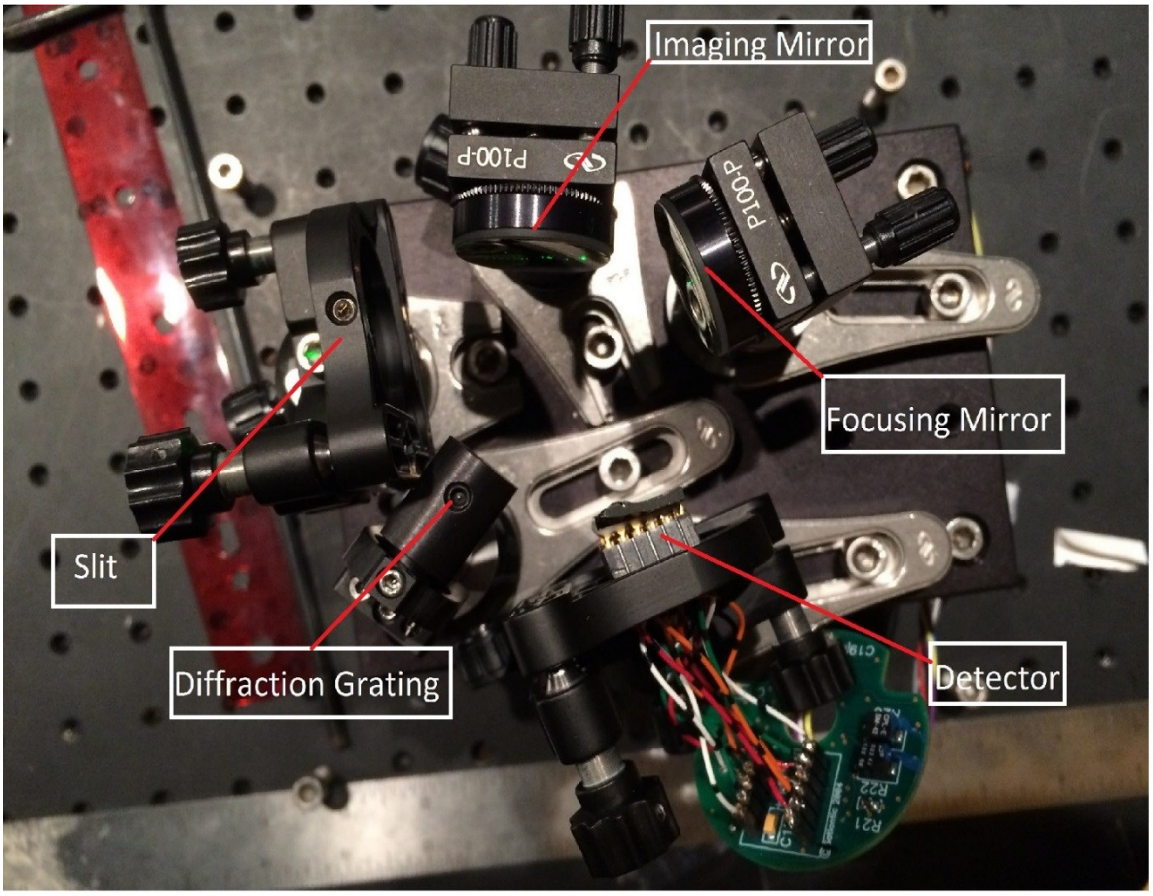

Figure 4.5 Optical bench setup

Once the setup was done, the next objective was the alignment of optics. We used Laser. Image 4.6 shows the alignment process. Before we used Laser, we mounted it so it would not have any tilt in both X and Y directions.

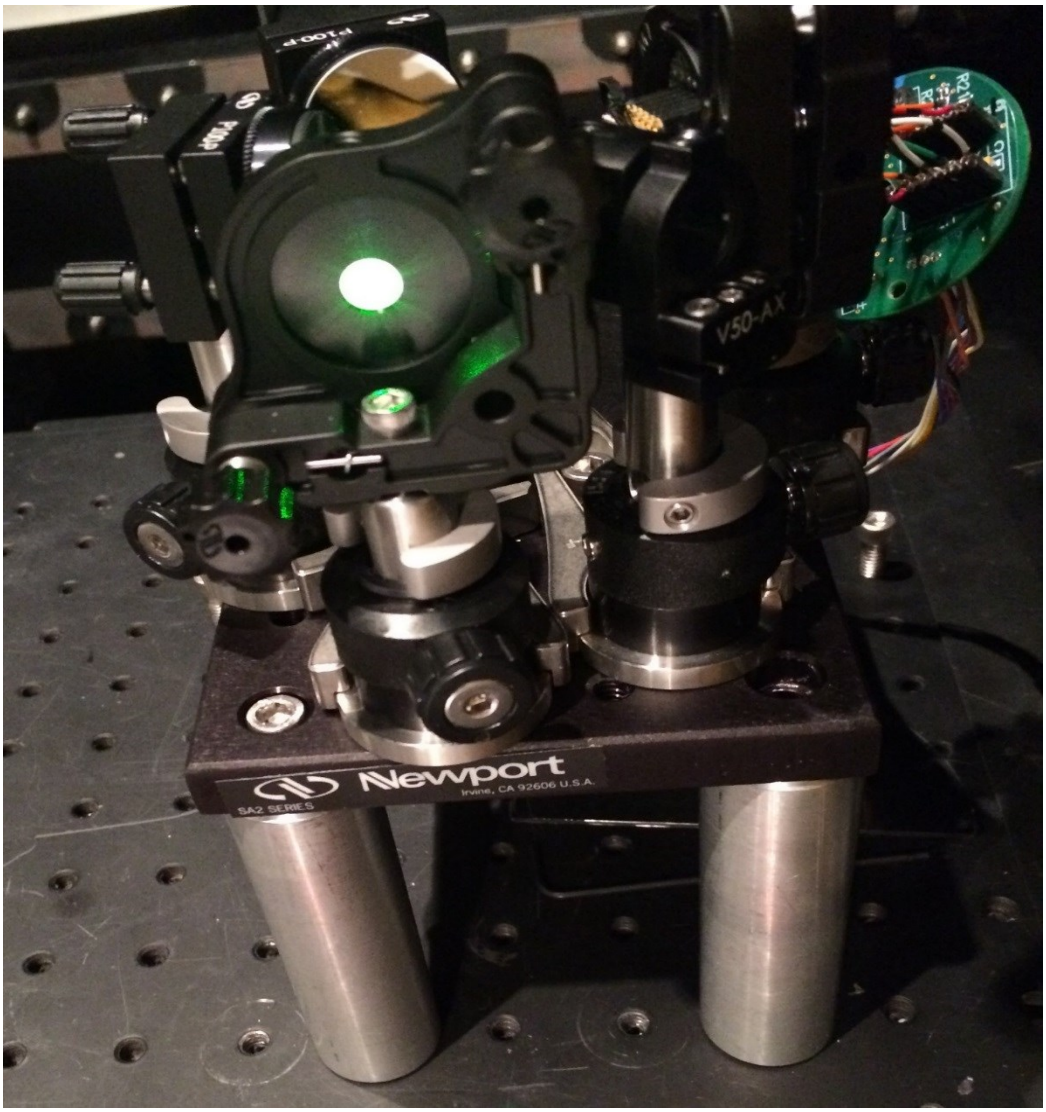

Figure 4.6 Alignment of Optics

4.4 Calibration Lamp

In this experiment, we used a Mercury argon lamp from Newport to check the output of the detector. This spectrometer is designed for UV wavelengths. This lamp has a known wavelength of 255nm. Figures 4.7 and 4.8 shows Mercury (Argon) lamp and its spectra, respectively. On the X-axis, we can see the wavelength range while the Y-axis represents light counts in percentage.

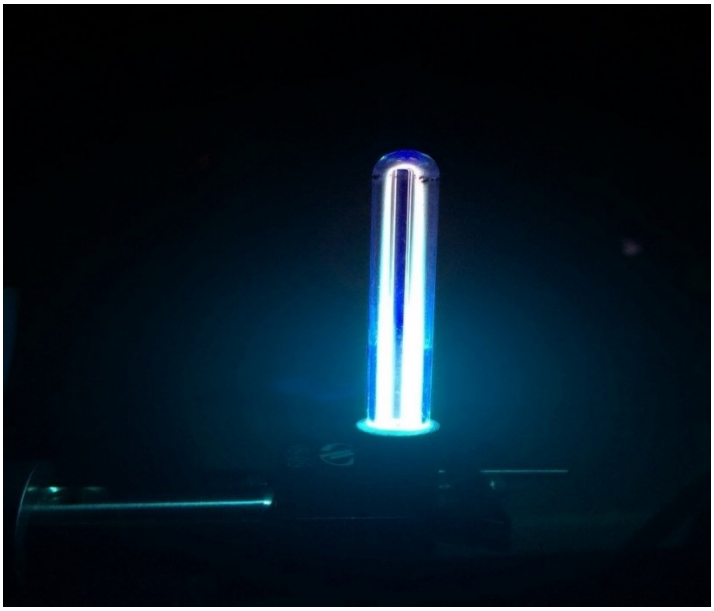

Figure 4.7 Mercury(Argon) lamp

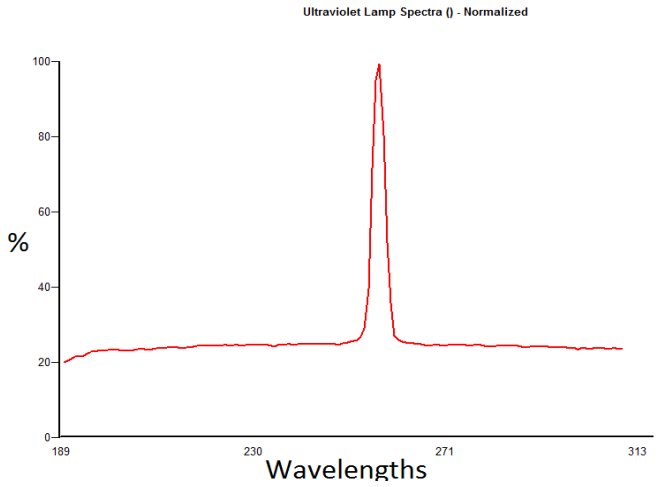

Figure 4.8 Mercury(Argon) lamp output in SetView

We can see from figure 4.8 that this spectrometer is able to detect the peak of the Hg(Ar) lamp. This design needs further improvement to block stray light in the system.

CHAPTER 5 Different tests of Spectrometer

For this chapter, we selected two spectrometers used in the industry and ran them through a series of tests to determine their characteristics. The tests were important to show that the requirements for the hyperspectral radiometer were met.

5.1 Polarization

To check polarization, we placed a polarizer in front of an optical fiber. We used an FEL lamp as our source because such a lamp produces a stable intensity with respect to time [30]. Figure 5.1 and 5.2 show the output of Spectrometers A and B. The data is plotted normalized to the average value from all polarizer positions to get polarization sensitivity.

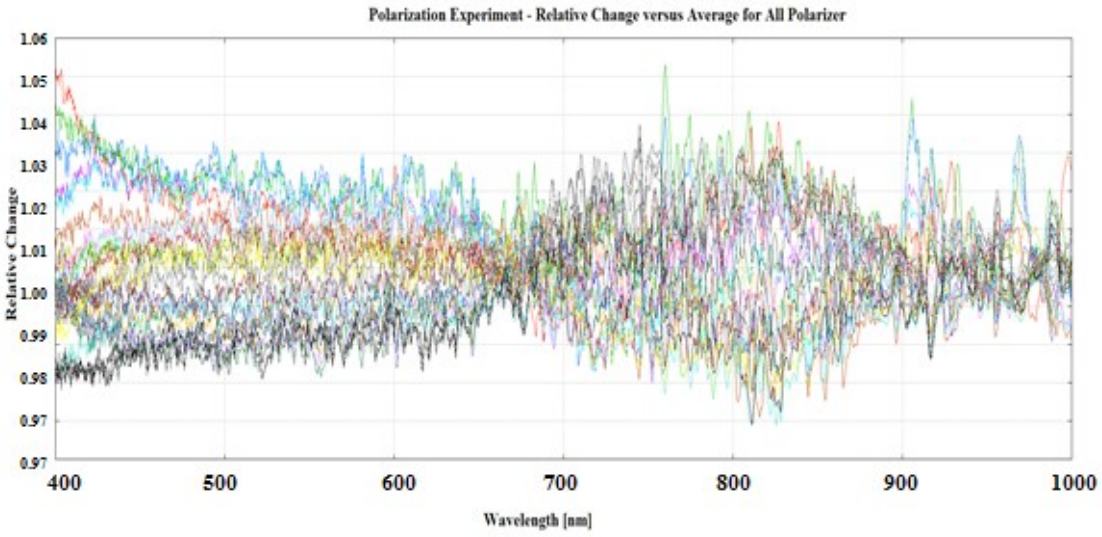

Figure 5.1 Spectra for each polarizer position, normalized to the average for all polarizer positions for Spectrometer A

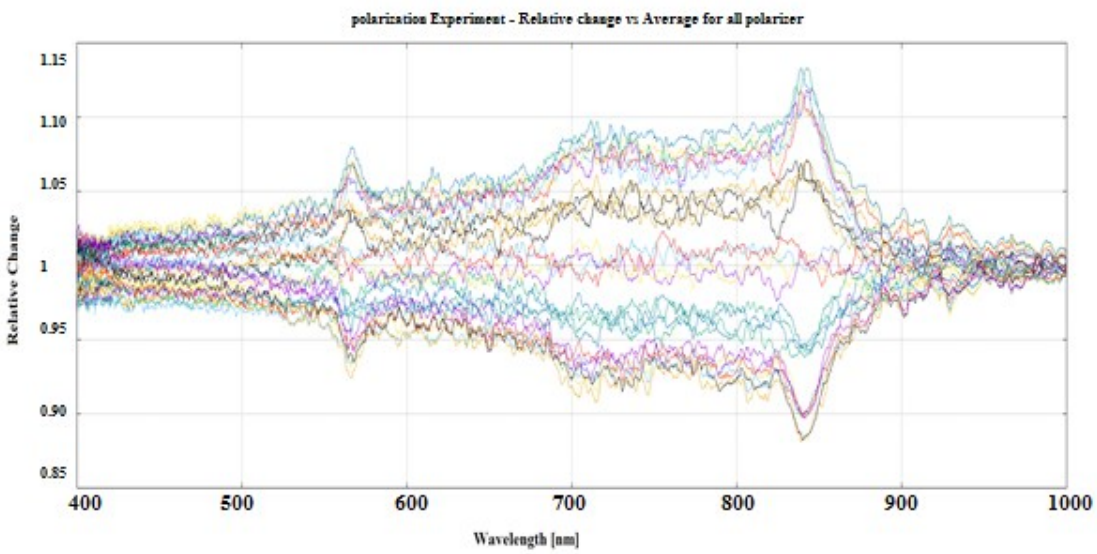

Figure 5.2 Spectra for each polarizer position, normalized to the average for all polarizer positions for Spectrometer B

We can see from the experiment results that Spec A has a relative change of 0.03 while Spec B is more sensitive to an average relative change of 0.05. We can say that both spectrometers are fairly sensitive to polarization. In Spectrometer B, we can see that the 830 nm to 850 nm wavelength range is slightly more sensitive to a relative change of more than 0.10. We wanted to check if we could decrease polarization without using a depolarizer. To do that, for one experiment, we roughened one side of the fiber. In the next experiment, we roughened both sides of the fiber. Figure 5.3 shows that result for the wavelength of 650nm. On the X-axis, the degree of polarization is shown while the Y-axis represents light counts.

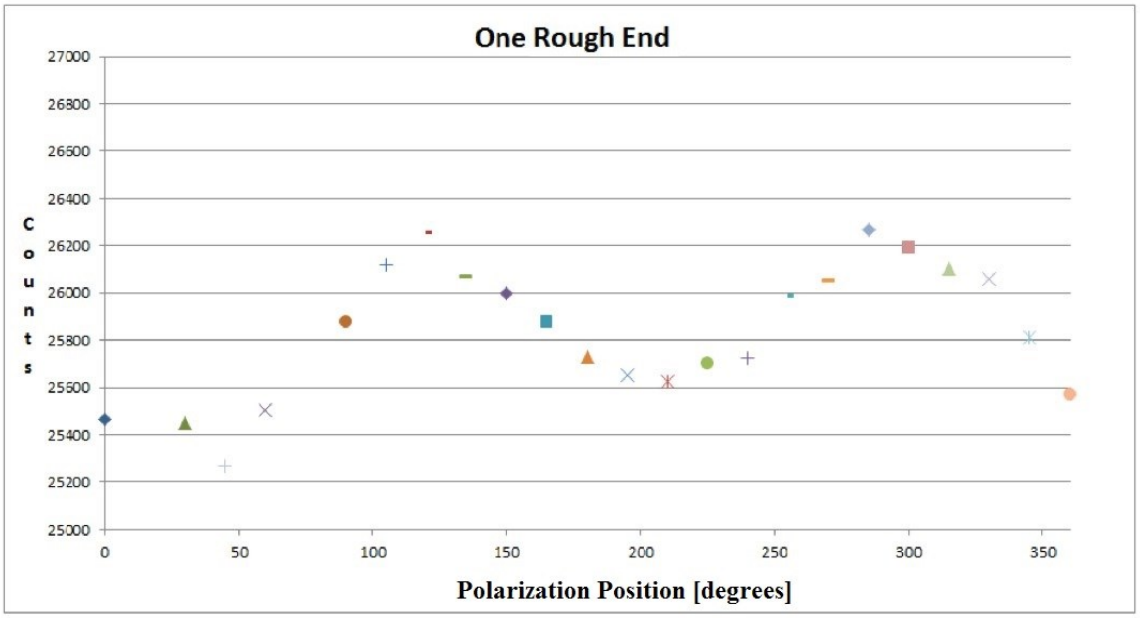

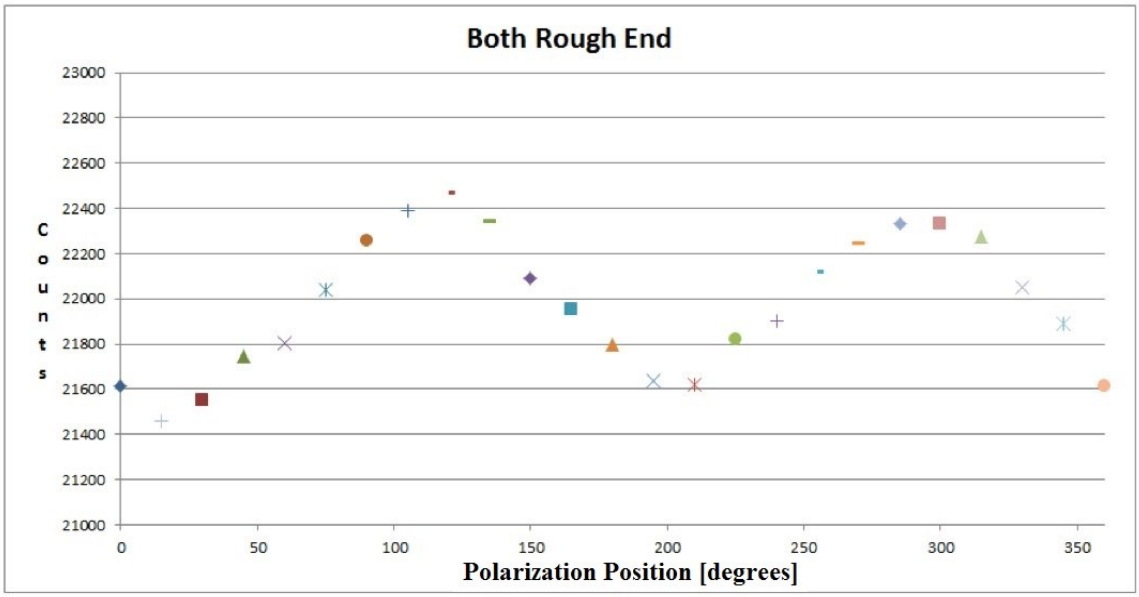

Figure 5.3 Polarization test with roughened fiber

From this graph, we can say that polarization sensitivity is less than 2%. It turns out fiber roughening did not work. We thought it did in one experiment but we cannot duplicate those results. We are now using a microretarder type depolarizer.

5.2 Warmup Test

In this experiment, we used an FEL lamp for a stable light source and collected data to check any changes over time [30]. For a measurement of dark counts, we blocked optical fiber input by using the electronic shutter. The following graph shows the light, the dark, and the light minus dark counts.

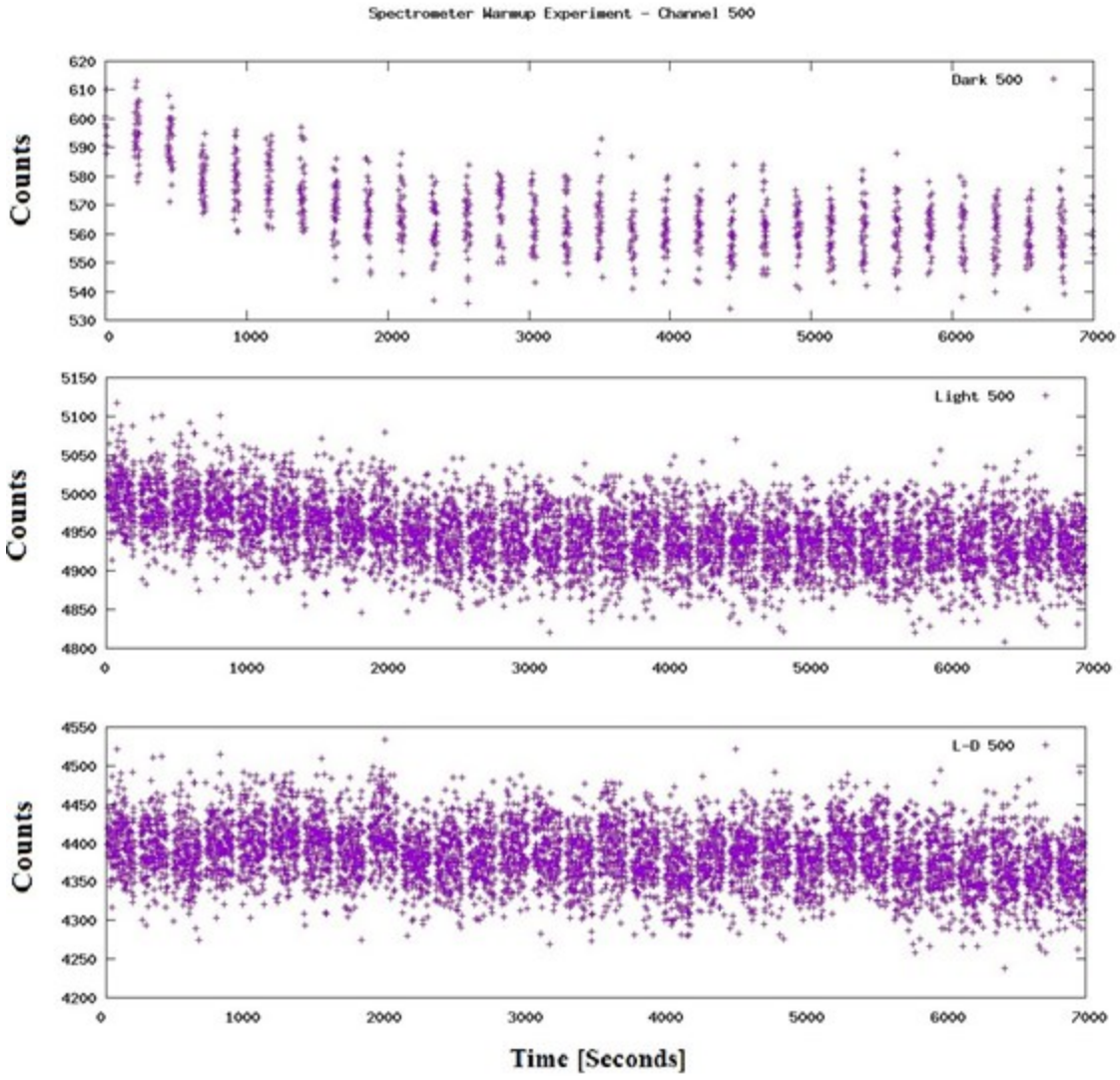

Figure 5.4 Spectrometer A warmup experiment – Channel 500

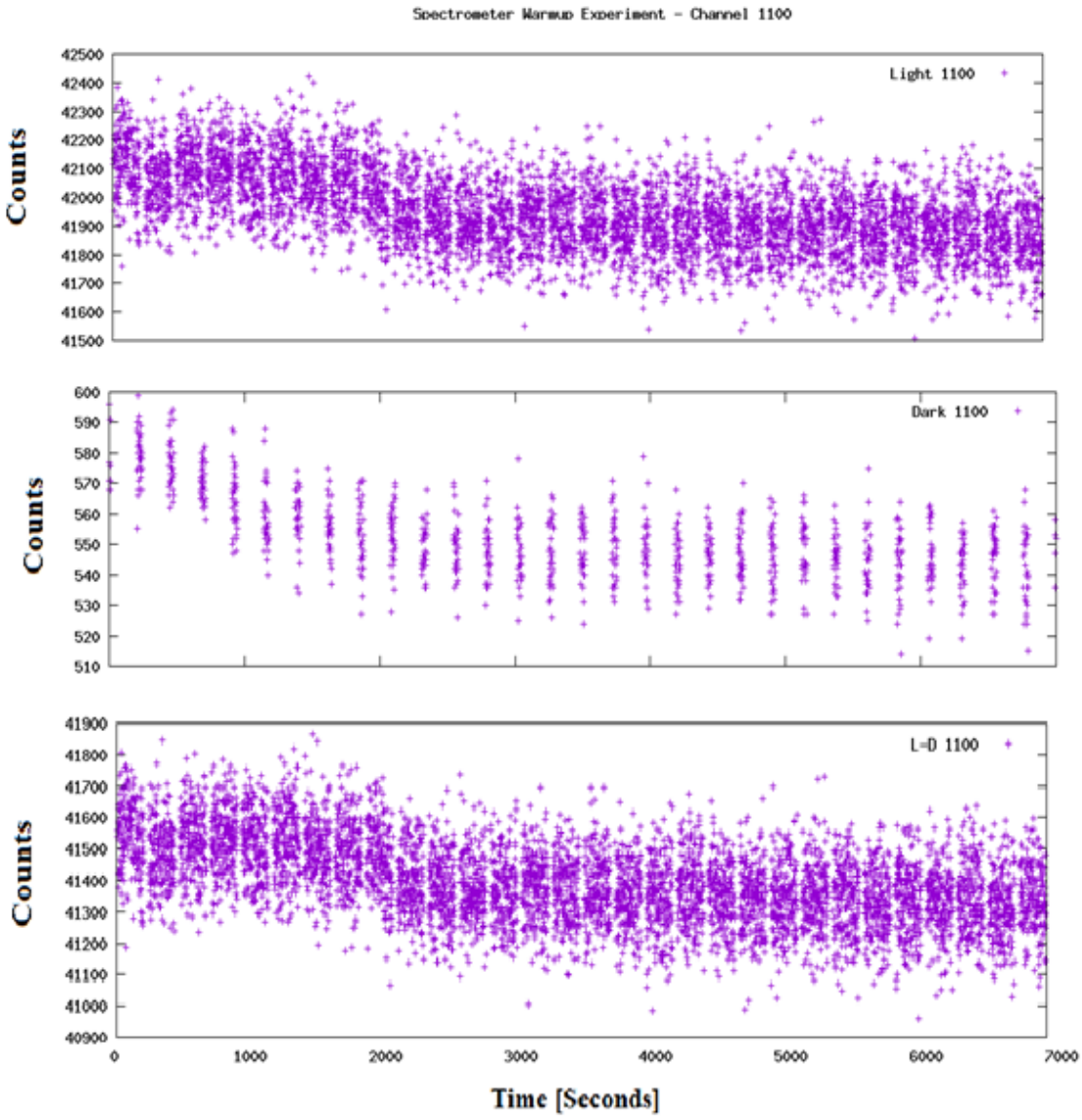

Figure 5.5 Spectrometer A warm up experiment – Channel 1100

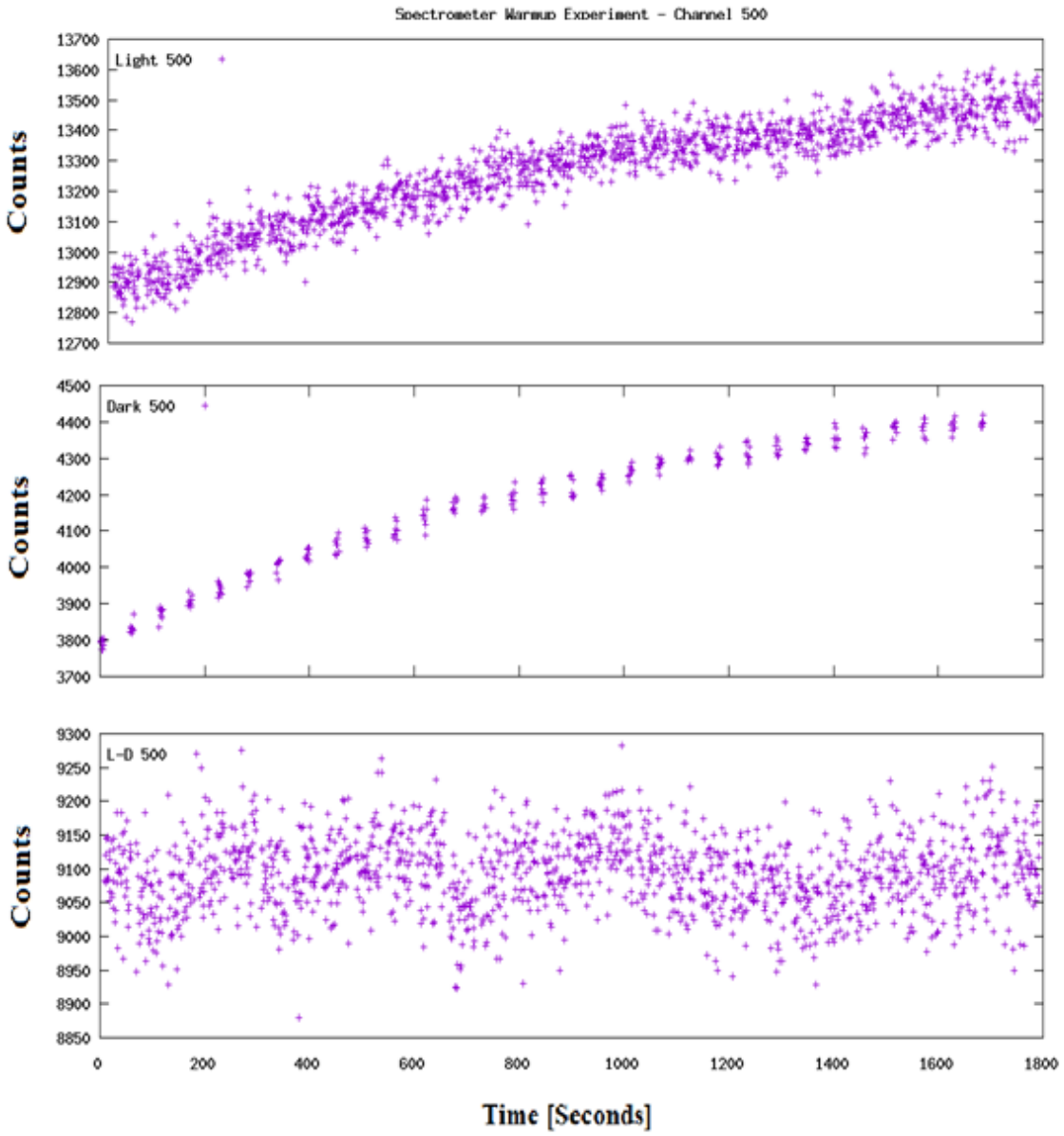

Figure 5.6 Spectrometer B warm up experiment – Channel 500

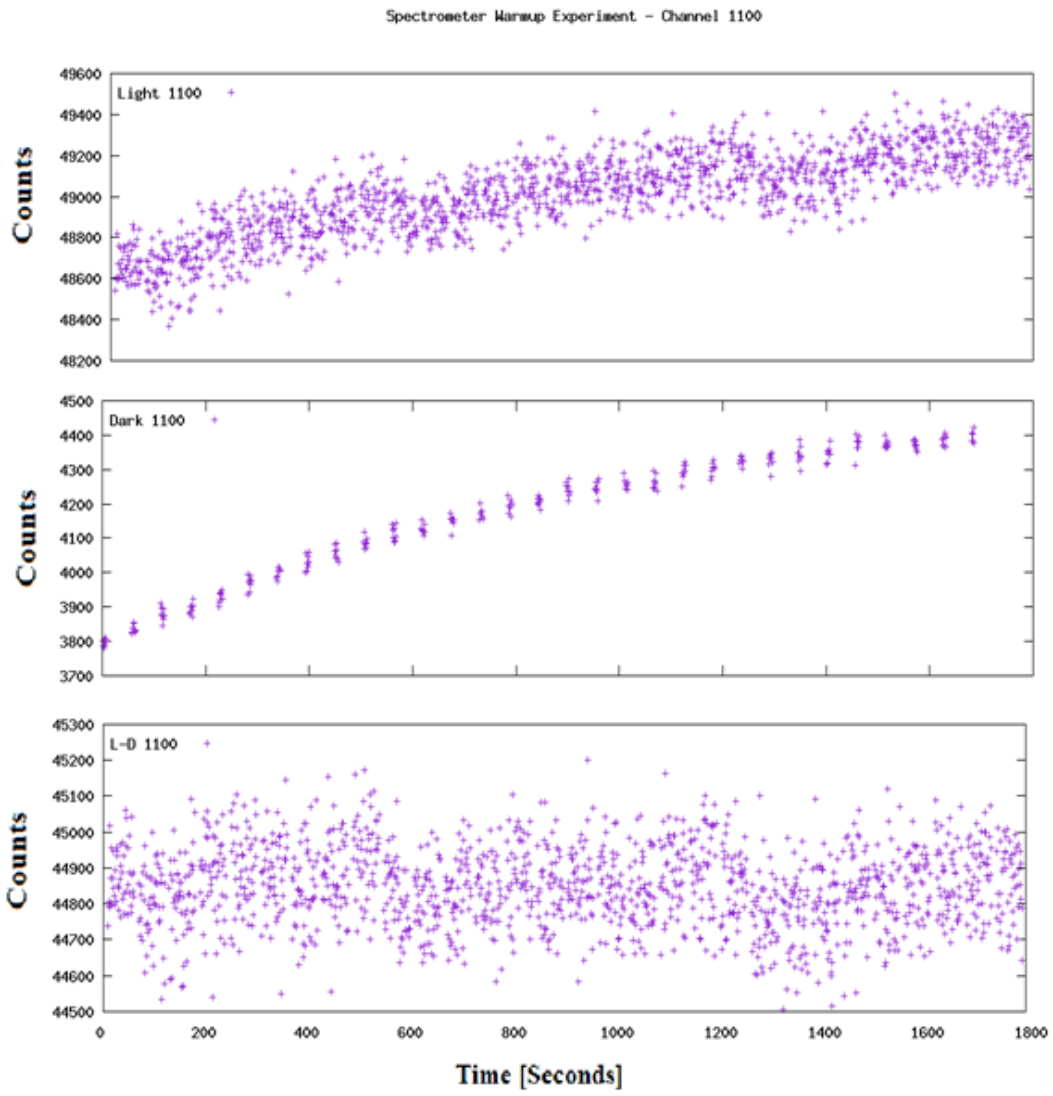

Figure 5.7 Spectrometer B warm up experiment – Channel 1100

Here we can see that light as well dark counts change over time. Just by looking at it, we can see for both light and dark, the change is 800 counts in 1800 sec. So we subtracted the dark counts from the light and found that the final counts were constant. In Spectrometer B, the dark counts are high (around 4K) so if we subtract L-D, there will be much lower counts. We used another mode of CCD to reduce the dark value. Refer to Chapter 2 for more detail about MPP.

5.3 Wavelength Accuracy and Mapping

The goals of this experiment were to verify the accuracy of the wavelength calibration provided by the manufacturer and to map the wavelength over the detector range to look for any discontinuities [30]. We decided the best way to do that was by using different calibration lamps. In Chapter 2, we showed the known spectrum of different calibration lamps that we used in this experiment.

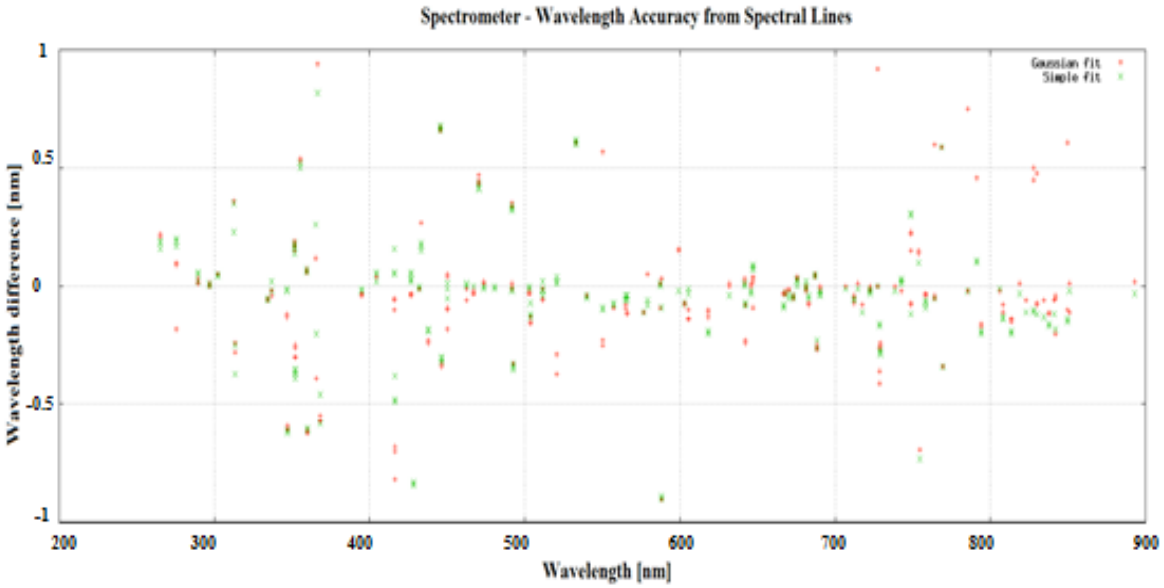

Figure 5.8 Wavelength Accuracy from spectral lines – Spectrometer A

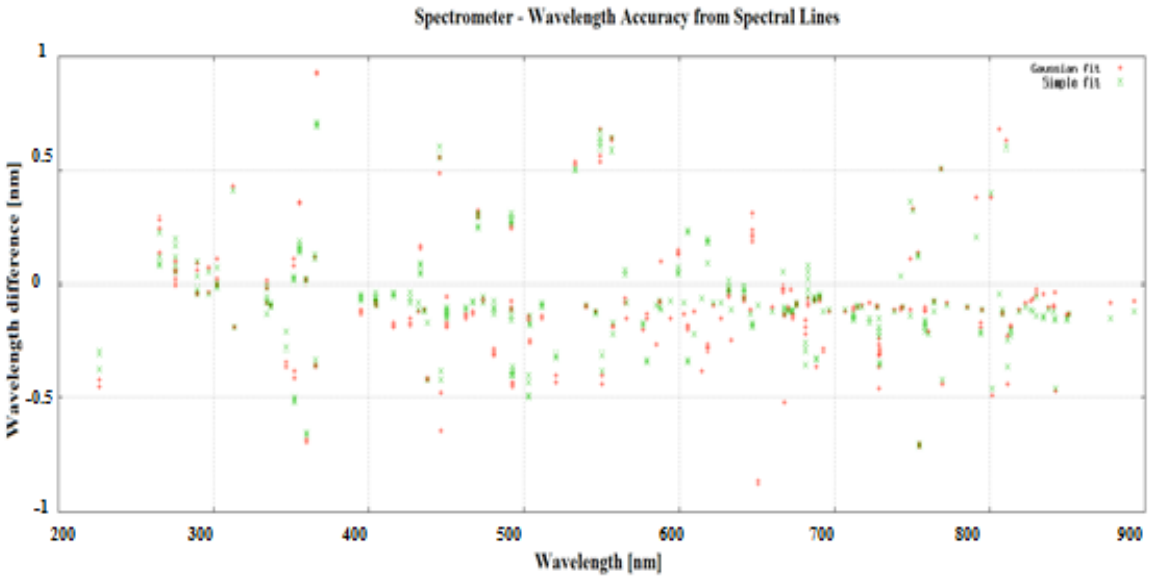

Figure 5.9 Wavelength Accuracy from spectral lines – Spectrometer B

Figure 5.11 and 5.12 contain a plot of peak differences from all the lamps. We compared all possible peaks of calibration lamps with actual spectrum captured by both spectrometers.

5.4 HeNe Laser Test

The aim of this test was to check for the presence of stray light in the system. We decided laser was the best option to do that. We used 632.8nm Helium-Neon laser for this experiment, as well as a simple glass filter to reduce the intensity of the light.

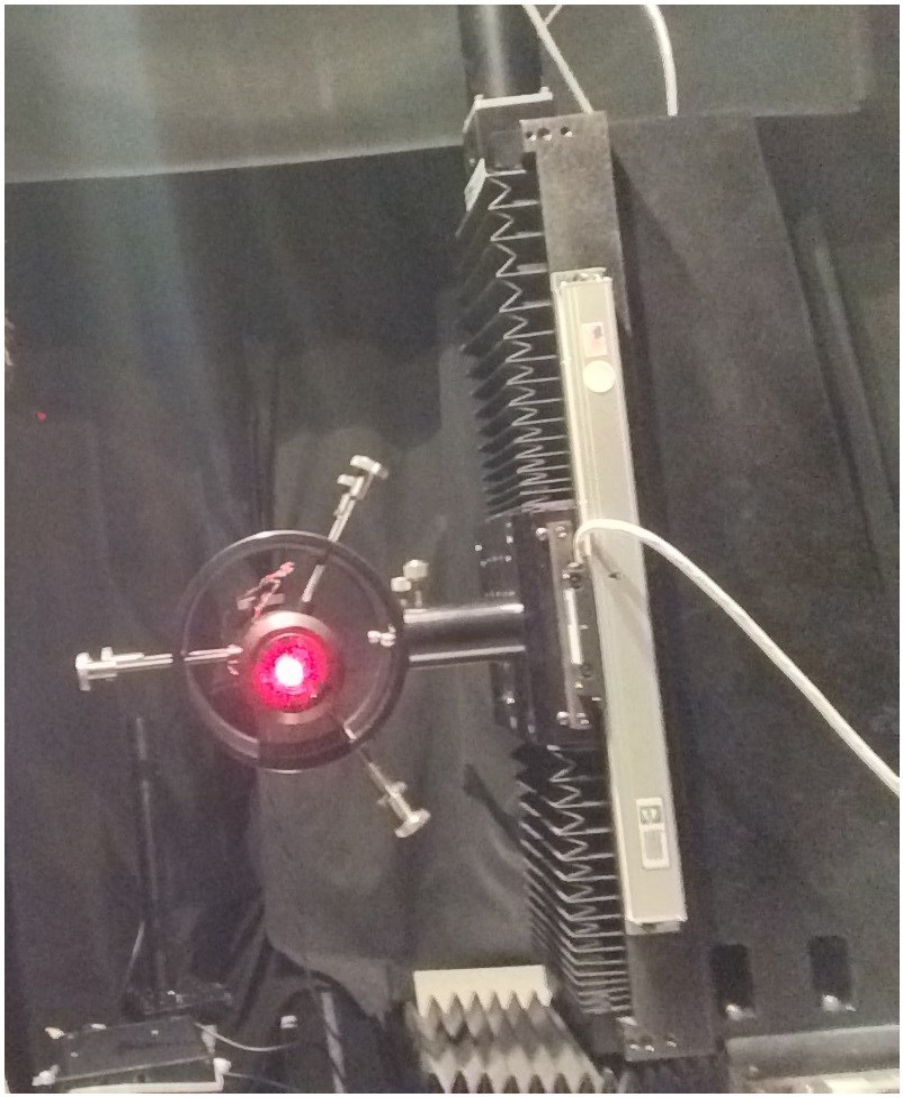

Figure 5.10 Actual HeNe Laser experiment

Figure 5.11 – 5.13 show the test results with different intensities for spec A.

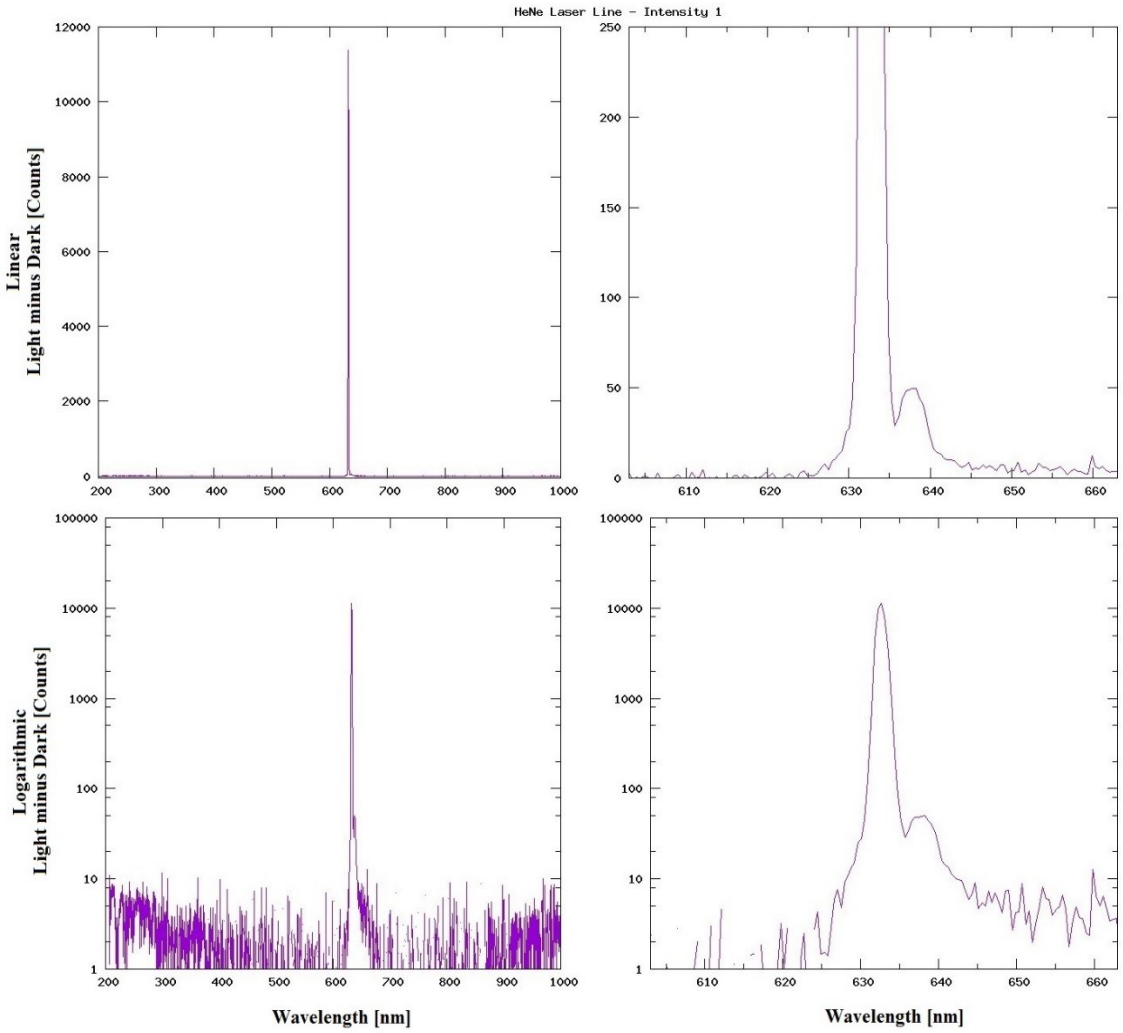

Figure 5.11 HeNe Laser Line. Low Intensity – Spectrometer A

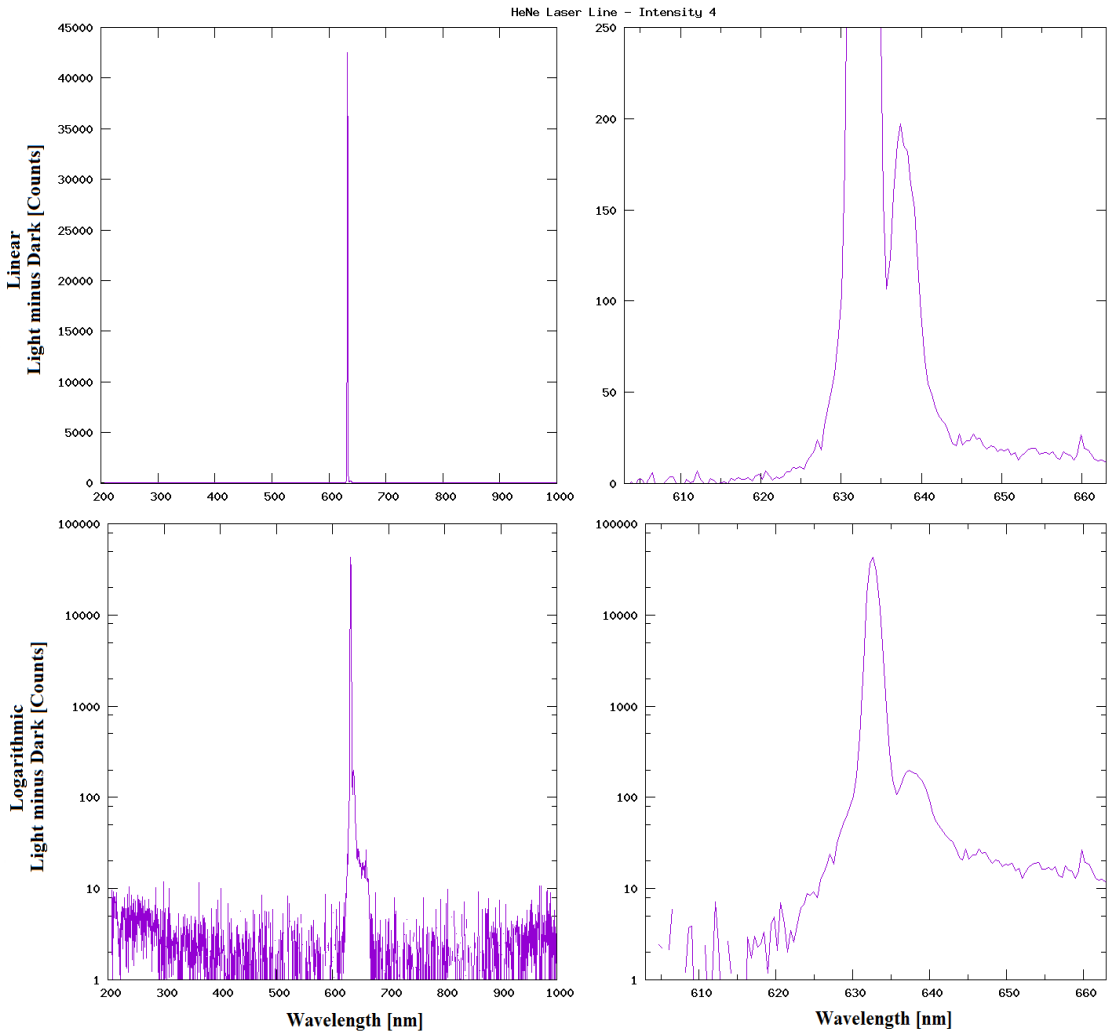

Figure 5.12 HeNe Laser Line. Medium Intensity – Spectrometer A

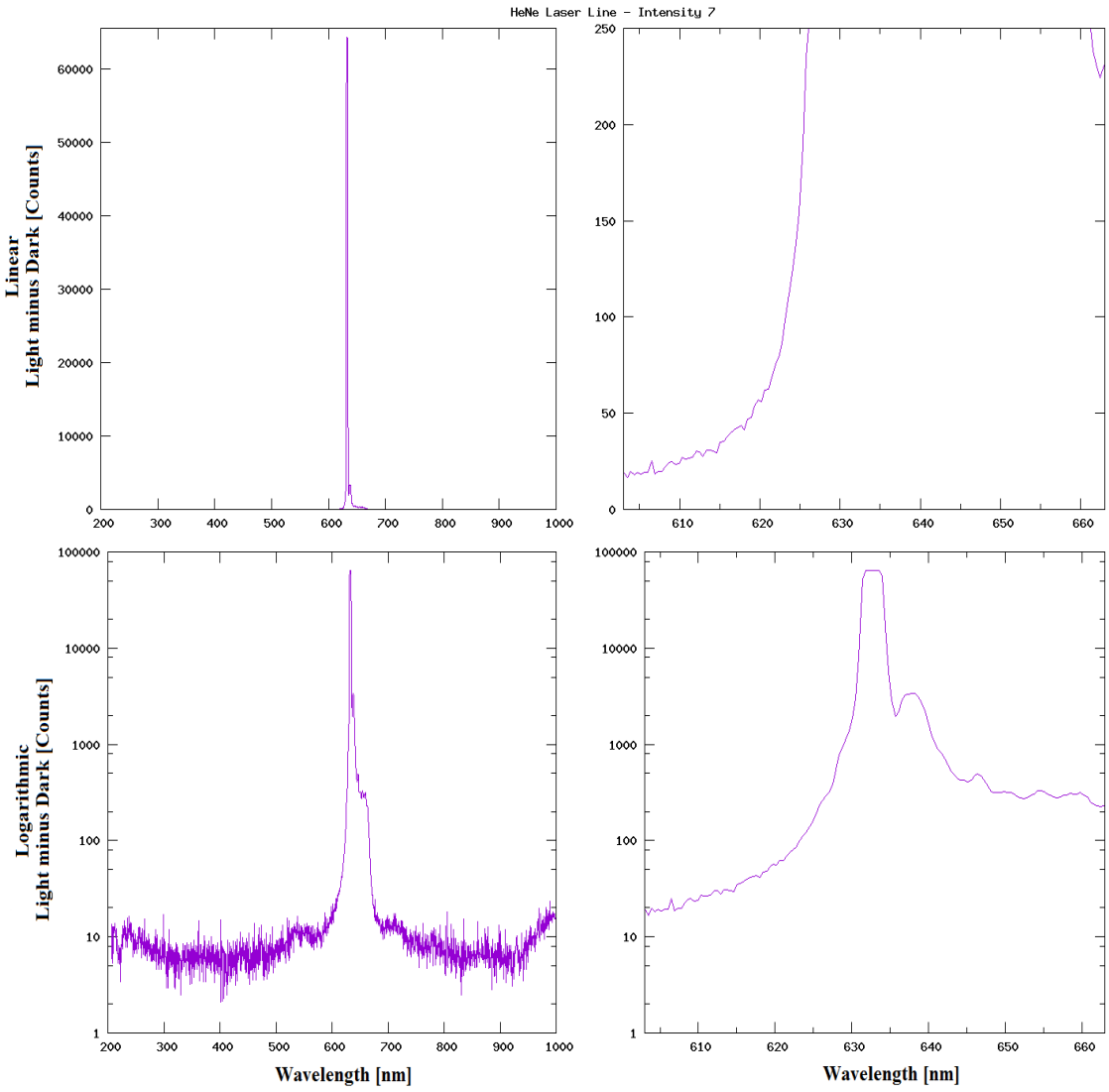

Figure 5.13 HeNe Laser Line. High Intensity – Spectrometer A

From the above results, we can conclude that Spectrometer A had a secondary peak centered at 638nm. We repeated the same experiment a couple of times, but there was no change. That may be due to the of stray light in the system. Figure 5.14 – 5.16 show the test results with different intensities for spec B.

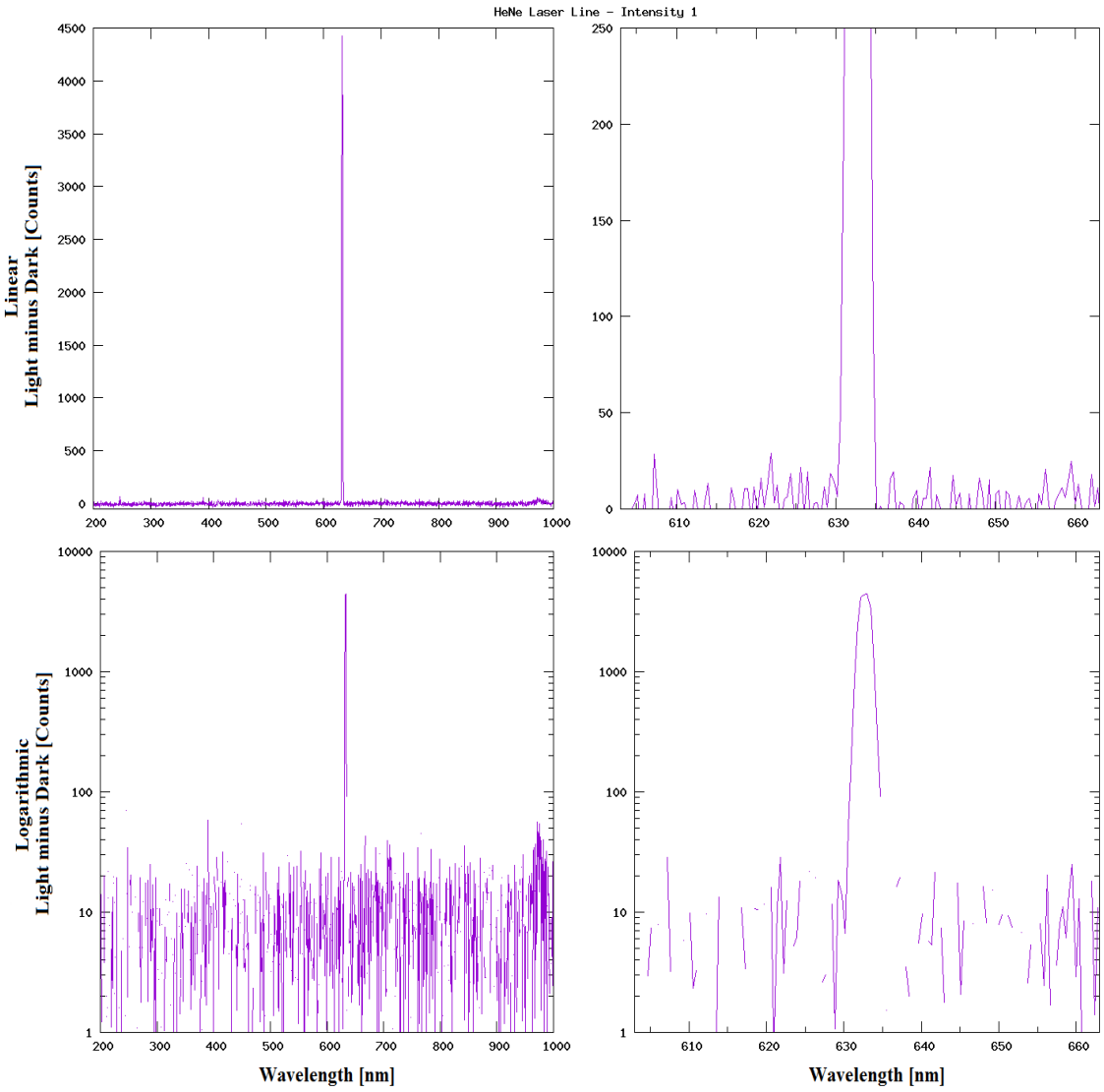

Figure 5.14 HeNe Laser Line. Low Intensity – Spectrometer B

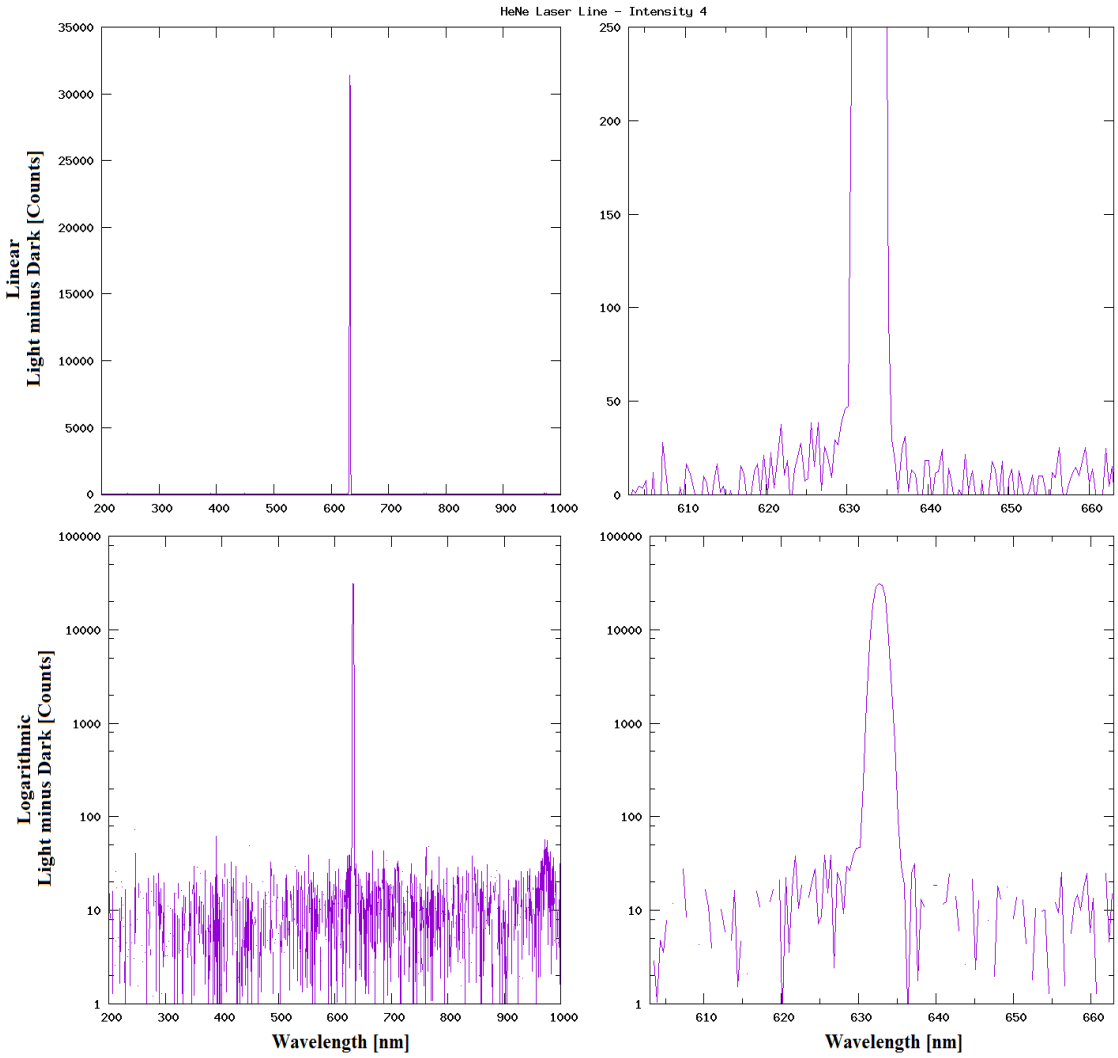

Figure 5.15 HeNe Laser Line. Medium Intensity – Spectrometer B

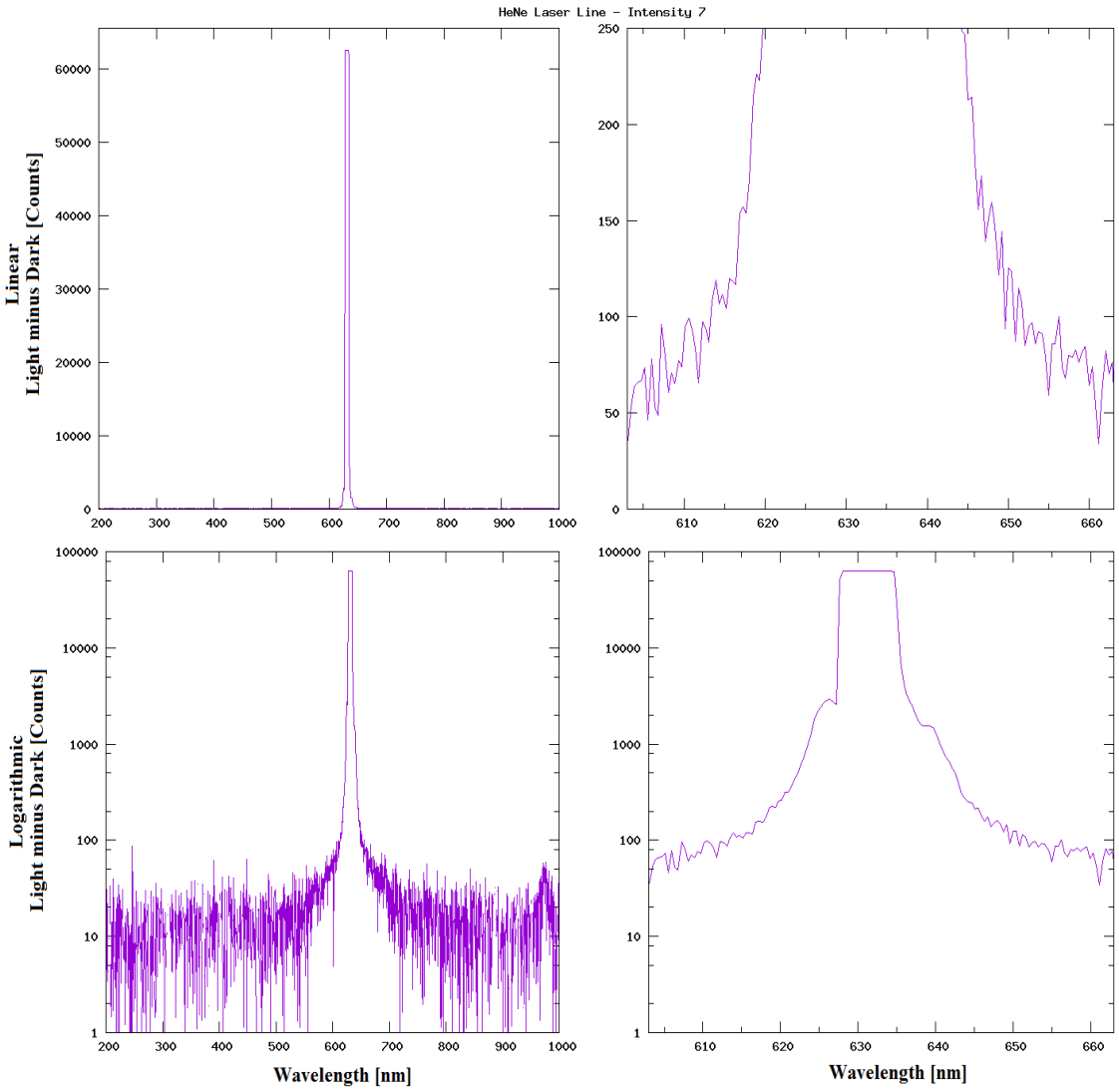

Figure 5.16 HeNe Laser Line. High Intensity – Spectrometer B

From the above results, we can see that both spectrometers had very good stray light levels, but the strange secondary peak in spec A is very bad and prevents us from performing a correction.

5.5 Thermal Test

The main purpose of this experiment was to check if the external temperature had any effect on data measurement of the spectrometer. We tested the temperature change effect in the range of 0° to 35° Celsius. To do that, we built one thermally insulated box and attached it to a liquid industrial chiller. By using the cooler, we could set any temperature we wanted. The pump inside the cooler circulated the coolant through the box.

One temperature sensor was attached to the body of the spectrometer to measure temperature. To check the temperature inside the box, we used SetView software that we installed on a laptop.

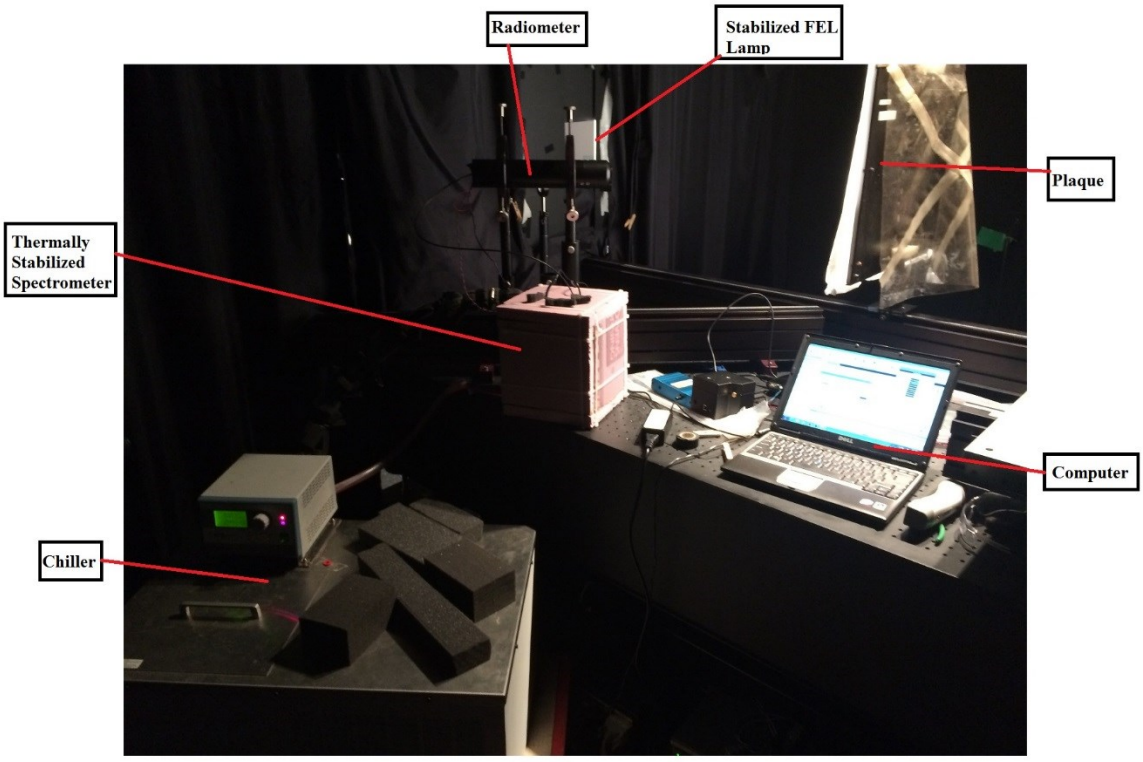

Figure 5.17 Actual thermal experiment setup

CHAPTER 6 Conclusion and Future work

This chapter summarizes the conclusion and lists future work to be carried out in this thesis.

6.1 Conclusion

In this thesis, we designed a small, low-cost UV spectrometer. We did all the necessary calculations and checked our design by using COMSOL Multiphysics and Zemax software. After that, we ordered all the necessary optics and holders to design and build an optical bench. Next, we aligned everything and used an Hg(Ar) pencil calibration lamp from Newport to check the output of the detector.

For the hyperspectral radiometer, we ran a number of different tests using two spectrometers to check their performance. Our test results showed that spectrometer B had a better optics design to block stray light in the system.

6.2 Future Work

For further development of the work carried out in this thesis, we can take the following steps:

1. Improve the current design of UV spectrometer to prevent stray light.
2. Use a UV source to calibrate a newly designed spectrometer
3. Build a prototype of a Hyperspectral Radiometer to measure field data

BIBLIOGRAPHY

[1] Nasagov. (2016). Nasagov. Retrieved 20 March, 2016, from http://neptune.gsfc.nasa.gov/osb/index.php?section=241

[2] Nasagov. (2016). Nasagov. Retrieved 20 March, 2016, from http://decadal.gsfc.nasa.gov/PACE/pace-2015/pacest13selections.pdf

[3] Sea-birdscientificcom. (2016). Sea-birdscientificcom. Retrieved 30 March, 2016, from https://sea-birdscientific.com/sites/default/files/resources/ocean_sciences_2016_poster_hypernav.pdf

[4] Confexcom. (2016). Confexcom. Retrieved 11 March, 2016, from https://agu.confex.com/agu/os16/preliminaryview.cgi/Paper92879.html

[5] SHI Chong,WANG Pucai,Teruyuki NAKAJIMA, et al. Effects of Ocean Particles on the Upwelling Radiance and Polarized Radiance in the Atmosphere-Ocean System. Adv. Atmos. Sci., 2015, 32(9): 1186-1196

[6] J. Strong, "The Johns Hopkins University and diffraction gratings," J. Opt. Soc. Am. 50, 1148-1152 (1960), quoting G. R. Harrison

[7] C. Palmer, Diffraction Grating Handbook (Newport Corporation, Rochester, NY, ed. 6, 2005).

[8] A. Labeyrie and J. Flamand, "Spectroscopic performance of holographically made diffraction gratings," Opt. Commun. 1, 5 (1969).

[9] S. Lindau, "The groove profile formation of holographic gratings," Opt. Acta 29, 1371-

[10] E. G. Loewen, M. Nevière and D. Maystre, "Grating efficiency theory as it applies to blazed and holographic gratings," Appl. Opt. 16, 2711-2721 (1977)

[11] Horibacom. (2016). Horibacom. Retrieved 18 March, 2016, from http://www.horiba.com/scientific/products/optics-tutorial/diffraction-gratings/

[12] M. C. Hutley and W. R. Hunter, "Variation of blaze of concave diffraction gratings," Appl.Opt. 20, 245-250 (1981).

[13] C. Palmer and W. R. McKinney, "Imaging theory of plane-symmetric varied line-spacegrating systems," Opt. Eng. 33, 820-829 (1994).

[14] H. A. Rowland, “Preliminary notice of the results accomplished in the manufacture and theory of gratings for optical purposes,” Philos. Mag. 13, 469 (1882)

[15] C. Palmer, “Theory of second-generation holographic diffraction gratings,” J. Opt. Soc. Am. 6, 1175-1188 (1989); T. Namioka and M. Koike, “Aspheric wavefront recording optics for holographic gratings,” Appl. Opt. 34, 2180-2186 (1995)

[16] Olympusmicrocom. (2016). Olympusmicrocom. Retrieved 13 April, 2016, from http://www.olympusmicro.com/primer/lightandcolor /polarization.html

[17] Satlanticcom. (2016). Satlanticcom. Retrieved 1 March, 2016, from http://satlantic.com/isus

[18] Photometricscom. (2016). Photometricscom. Retrieved 8 April, 2016, from http://www.photometrics.com/resources/learningzone/mppmode.php

[19] Newportcom. (2016). Newportcom. Retrieved 15 August, 2015, from http://www.newport.com/Calibrated-Sources/378236/1033/info.aspx

[20] Newportcom. (2016). Newportcom. Retrieved 8 March, 2016, from http://www.newport.com/Pencil-Style-Calibration-Lamps/377846/1033/info.aspx

[21] Shafer, L. Megil and L. Droppelman, “Optimization of Czerny-Turner spectrometers,” J. Opt.Soc. Am. 54, 879-888 (1964);

[22] J. M. Simon, M. A. Gil and A. N. Fantino, “Czerny-Turner monochromator: astigmatism in the classical and in the crossed beam dispositions,” Appl. Opt. 25,3715-3720 (1986);

[23] K. M. Rosfjord, R. A. Villalaz and T. K. Gaylord, “Constant-bandwidth scanning of the Czerny-Turner monochromator,” Appl. Opt. 39, 568-572 (2000)

[24] Mass Spectrometry: A Textbook by Jürgen Gross. Springer, 2010. A fully illustrated reference covering the chemistry and theory of mass spectrometry more than the applications

[25] Comsolcom. (2016). COMSOL Multiphysics©. Retrieved 12 February, 2016, from https://www.comsol.com/video/what-is-comsol-multiphysics

[26] Wikipediaorg. (2016). Wikipediaorg. Retrieved 11 February, 2016, from https://en.wikipedia.org/wiki/COMSOL_Multiphysics

[27] "COMSOL Multiphysics Modeling Software". COMSOL.com. Comsol, Inc. Retrieved 20 November 2015.

[28] Physicsluse. (2016). Physicsluse. Retrieved 10 October, 2015, from http://www.atomic.physics.lu.se/fileadmin/atomfysik/Biophotonics/Education/MultiphysicsExercise.pdf

[29] Zemaxcom. (2016). Zemaxcom. Retrieved 7 September, 2015, from http://www.zemax.com/zmx/company/about

[30] Ronnie Van Dommelen, personal communication, 2015